NATIONAL ADVISORY COMMITTEE FOR AERONAUTICS

WARTIME REPORT

ORIGINALLY ISSUED
June 1945 as
Memorandum Report L5E09a

ESTIMATION OF THE PERFORMANCE AND LONGITUDINAL STABILITY AND CONTROL OF A LIFTING-BODY TYPE OF CARGO AIRPLANE FROM TESTS OF SIMPLIFIED MODELS

By D. Feigenbaum

Langley Memorial Aeronautical Laboratory
Langley Field, Va.

WASHINGTON

MR No. L5E09a

NATIONAL ADVISORY COMMITTEE FOR AERONAUTICS

MEMORANDUM REPORT

for the

Army Air Forces, Air Technical Service Command

ESTIMATION OF THE PERFORMANCE AND LONGITUDINAL STABILITY AND CONTROL OF A LIFTING-BODY TYPE OF CARGO AIRPLANE FROM TESTS OF SIMPLIFIED MODELS

By D. Feigenbaum

SUMMARY

Tests were made in the Langley stability tunnel to compare the drag of airplane configurations having conventional bodies with that of an airplane configuration intended to carry cargo in a detachable airfoil-shaped body. The results of these tests are presented graphically. An analysis of the performance and longitudinal stability and control characteristics of a lifting-body cargo airplane is also presented, and this type is compared with a more conventional cargo airplane.

Comparison of the polars obtained by the analysis with the experimental results obtained for a specific model shows that the methods used will give reasonably good comparative performance estimates. Although the specific assumptions used may be open to question, the comparison of the proposed design with a conventional airplane indicates the practicability of the design. No further investigation of the general aerodynamic characteristics of the lifting-body type of airplane is considered necessary.

INTRODUCTION

At the request of the Army Air Forces, Air Technical Service Command, a preliminary investigation of the drag of several configurations of a lifting-body cargo airplane was conducted in the Langley stability tunnel.

In order to investigate the aerodynamic characteristics of such a cargo airplane, an analysis was made of the performance and of the longitudinal stability and control characteristics of a specific design. The methods used and assumptions involved in the analysis are presented in the appendices. The stability and control analysis considered mainly the effect of body location and center-of-gravity location on the tail area required.

COEFFICIENTS AND SYMBOLS

The coefficients and symbols used in this report are defined as follows:

L lift

D drag

M pitching moment measured about quarter-chord point

C_L lift coefficient $= \frac{L}{qS}$

C_D drag coefficient $= \frac{D}{qS}$

C_{D_o} profile-drag coefficient

C_m pitching-moment coefficient about quarter-chord point $= \frac{M}{qSc}$

C_{m_o} pitching-moment coefficient at zero lift

S projected area

S' wing area not covered by cargo body $S = kS'$

S'' projected area of test models

c chord

b span

l distance of tail quarter-chord point from wing quarter-chord point

a distance of body quarter-chord point ahead of wing quarter-chord point

x distance of center of gravity behind wing quarter-chord point

x_n distance of neutral point behind wing quarter-chord point

$\bar{x}$ distance of center of gravity behind cargo body quarter-chord point

R flight range

hp horsepower

A aspect ratio

W weight

W_f weight of fuel

f fuel consumption rate

q dynamic pressure $= \frac{1}{2}\rho V^2$

V airspeed

ρ air density

η engine-propeller efficiency

α angle of attack

α_o section angle of attack

α_i induced angle of attack

$\Delta\alpha_f$ effective change in angle of zero lift due to flap deflection

C_{L_α} $\frac{dC_L}{d\alpha}$

δ angle of deflection of flap or control surface

i angle of incidence

ϵ downwash angle at tail

Subscripts:

b refers to cargo body

c + b refers to cargo body and booms

t refers to horizontal tail

s refers to vertical tail

f refers to flap

c refers to cargo

n refers to engine nacelles

e refers to airplane with cargo body off

w refers to wing, when used, otherwise wing parameters have no subscripts

m refers to scale model

1 refers to the spanwise portion of wings without flaps

2 refers to the flapped spanwise portion of the wing outside the slipstream

3 refers to the spanwise portion of the wing in the slipstream

MODELS

Tests were made on simplified models representing several configurations of a cargo airplane using a large-chord short-span airfoil-shaped body and twin booms. The body had a section with a 0.25c maximum thickness at 0.40c and a maximum camber of 0.02c at 0.40c; the chord c was 30.2 inches and the span was varied; 4-, 12-, and 22-inch spans were tested. The body-boom combinations, body alone, and booms alone were tested on the wings. In one of the tests of the booms, the wing chord between the booms was increased by extending the leading edge 23 percent. For comparison, tests were also made on more conventional bodies; one of 5- by 7.55-inch rectangular cross section, and another of 6-inch-diameter circular cross section,

geometrically similar to the fuselage of the Douglas C-74. The conventional bodies have cargo capacities approximately equal to that of the 4-inch cargo body. Illustrations of these models are shown in figures 1, 2, 3, 4, and 5.

All the bodies were tested on the same 12-inch-chord dural airfoil of NACA 4318 section, which completely spanned the tunnel. The cargo-body models were mounted so that their quarter-chord points were 6.58 inches ahead of the wing quarter-chord point. The right end of the airfoil passed through the tunnel wall and was fastened to the balance frame outside the tunnel. The gap around the wing where it passed through the tunnel wall was about 1/16 inch wide. The left end of the airfoil came almost to the tunnel wall, leaving approximately a 1/16-inch gap between the wing and the wall. This end of the airfoil was mounted on the balance frame by means of a shaft which was fastened to the end of the wing and passed through the tunnel wall. The construction of the wing and mount can be seen in figure 2, and a model with the same configuration as shown in figure 2(a) is shown mounted in the tunnel in figure 5.

TESTS AND RESULTS

The tests were made in the 6- by 6-foot test section of the Langley stability tunnel at a constant dynamic pressure q of 64.3 pounds per square foot, corresponding to a Reynolds number of 1.44×10^6 based on the 1-foot wing chord. Measurements were made of lift, drag, and pitching moments. The data were corrected for tunnel-wall effects and are presented in standard NACA coefficient form.

The results of the tests are shown in figures 6 through 16. A résumé of the tests and results is given in the following table:

Model configuration	Figure no.
Wing alone	6
Wing + 22-inch cargo body + booms Wing + 12-inch cargo body + booms Wing + 4-inch cargo body + booms } $i_w = 0^\circ$	7
Wing + 22-inch cargo body + booms, $i_w = 0^\circ, 2\frac{1}{2}^\circ, 5^\circ$	8
Wing + 22-inch body Wing + 12-inch body Wing + 4-inch body } $i_w = 0^\circ$	9
Wing + booms at 22-inch spacing constant chord wing Wing + booms at 12-inch spacing constant chord wing Wing + booms at 4-inch spacing constant chord wing } $i_w = 0^\circ$	10
Wing alone Wing + 12-inch cargo body + booms Wing + 12-inch cargo body Wing + booms at 12-inch spacing constant chord wing Wing + booms at 12-inch spacing increased chord wing between booms } $i_w = 0^\circ$	11
5-inch conventional body, $i_w = 0^\circ$	12
Circular body, high wing, $i_w = 0^\circ, 2\frac{1}{2}^\circ, 5^\circ$	13
Circular body, low wing, $i_w = 0^\circ, 2\frac{1}{2}^\circ, 5^\circ$	14
Wing alone Wing + 4-inch cargo body + booms Wing + 5-inch conventional body Wing + circular body, high wing Wing + circular body, low wing } $i_w = 0^\circ$	15
Wing + 22-inch cargo body + booms Wing + 22-inch cargo body + booms extended T.E. } $i_w = 0^\circ$	16

The tests on the wing alone can be considered as two-dimensional tests, and the data in figure 6 are section data. The other tests are of three-dimensional bodies superimposed on a two-dimensional wing.

The data presented in figures 8 and 13 cannot be compared directly with the other data presented, since the tests from which the results on these two figures were obtained were run with the gap around the wing at the tunnel wall sealed. These two figures are comparable only within themselves to show the effects of wing incidence. All other data were obtained with the gap around the wing unsealed.

DISCUSSION

Test Data

The drag data from the tests were broken up into several components to determine where the drag could be reduced. All the drag coefficients were based on the wing area of 6 square feet. Figure 17 shows the values of minimum drag coefficient of the various components of the cargo airplane. The variation of the cargo-body drag increment with body width (from fig. 9) was not zero when extrapolated to zero body width. The skin friction of the sides of the cargo body was calculated at a Reynolds number based on the test airspeed and body chord, assuming a turbulent boundary layer on the body sides. The computed skin-friction drag coefficient coincided with the drag increment at zero body width.

From the tests of the booms alone on the wings (see fig. 10), the drag of the booms was found to be independent of the boom spacing. Also, there seemed to be no drag interference between the booms and cargo body, because the increment of drag added by the booms was the same whether or not the cargo body was present. This can be seen clearly in figure 17.

Tuft studies were made and showed that the flow at the trailing edge of the airfoil-section cargo body was always separated. The flow on the upper surface was separated to some extent near the trailing edge even at -8° angle of attack. This separated flow occurred on the body when tested either with or without the booms. In

an attempt to eliminate the flow separation, the cargo-body length was increased 10 percent by extending the trailing edge as shown in figure 1, thereby reducing the trailing-edge angle from 50° to about 30°. Tuft tests showed that this modification eliminated the flow separation on the upper surface for the negative angle-of-attack range, and made it less widespread for small positive angles of attack. Force tests showed that the drag was decreased in the minimum drag range. The results of these force tests are shown in figure 16.

In figure 11, it can be seen that the booms have some interference effect on the pitching moments of the cargo body. Adding the booms to the wing and cargo-body combination produced a pitching-moment increment greater than that produced by adding the booms to the wing alone. This is probably a result of the interference effects between the forward portion of the cargo body and the large portion of the booms extending in front of the cargo body.

Analysis

The data were applied to an analysis of the performance and the longitudinal stability and control characteristics of a full-size cargo airplane utilizing the airfoil-shaped cargo body. However, no attempt was made to estimate the control forces. The specific design chosen for analysis was suggested by Col. C. F. Greene, Liaison Officer between the Air Technical Service Command and the Langley Laboratory of the National Advisory Committee for Aeronautics. The characteristics of the airplane are as follows:

The airplane considered is a four-engine high-wing cargo carrier, designed to accommodate bulky and heavy equipment and material. The body for carrying the cargo, which is detachable for simple and rapid loading and unloading, has an airfoil-shaped longitudinal section. The remaining portion of the airplane is a complete flyable unit in itself. A three-view drawing of the basic airplane is shown in figure 18, and the main dimensions are listed in table I.

The methods used in the analysis and the values assumed or estimated for the various parameters are given in appendix A. An analysis of the test data to justify some of the assumptions made is given in appendix B.

The values given in table II and in figures 19 through 22 are only approximations, since the drag data were estimated, or taken from low Reynolds number tests of a simple body and boom combination mounted on a constant-chord wing which completely spanned the wind tunnel. In order to justify the method used in estimating the drag characteristics, a lift-drag polar was estimated for the Douglas C-74, using the test data in figure 14 for the model with the circular fuselage and low wing at $2\frac{1}{2}^{\circ}$ incidence. In figure 19, this polar is compared with data obtained from tests of a complete C-74 model. The comparison between the computed and measured drags of the C-74 indicates that the method of estimating the drag is satisfactory.

Performance.- The drag of the complete airplane was estimated, as shown in appendix A, from the test data, with a suitable allowance made for the decrease in drag when booms not extending in front of the body are used. The estimated lift-drag polars for the complete airplane, and the airplane with the cargo body removed and the drag equivalent of flat plates of 0-, 50-, and 100-square-foot areas placed between the booms to represent large items of cargo hung from the wing but not enclosed in the body, are shown in figure 20.

It is desirable to compare the lifting-body type of airplane with a more conventional cargo airplane in order to show their relative performance. The C-74 cargo airplane, however, cannot be used for this comparison because the sizes and wing loadings are different for the two airplanes. In order to compare the two types of airplane on the same basis, the polar was estimated for an airplane with a fuselage similar to that of a C-74, but with a cargo volume, gross weight, and wing size and plan form the same as those of the lifting-body design. The drag coefficients of the airplane are compared with those of the lifting-body airplane in figure 20. The minimum drag coefficient of this comparison airplane was slightly lower than that of the complete cargo airplane (0.0223 as compared with 0.0237).

Power required versus speed curves were drawn from the estimated lift-drag polars. A power available versus speed curve for normal rated power (8800 bhp) was estimated from the engine-propeller characteristics. The estimated power curves and a curve showing the power required to overcome the induced drag at a wing loading of 40 pounds per square foot is shown in figure 21.

Also shown is the power required for the large conventional type of airplane for comparison. This conventional type is the one mentioned previously, which has a fuselage similar to that of the C-74 but with its weight and wings the same as those of the lifting-body cargo airplane.

The sea-level performance of the cargo airplane was estimated from the power curves for three conditions: body on, design gross weight; body on, light load (as at the end of a long-range flight); and body off, light load. The cargo load versus range characteristics at constant brake horsepower and at constant lift coefficient, which are presented in the form of curves in figure 22, were estimated from the power curves and fuel consumption data of the engine at minumum horsepower required (4760 bhp) and at 6000 bhp and at the maximum lift-drag ratio. Flight at the maximum lift-drag ratio represents the most efficient flying conditions, and the maximum range for any loading may be attained by this method. However, it is easier for the pilot to fly at constant brake horsepower, since this requires a single throttle setting and no adjustments of power during flight.

The landing speed was also estimated. The maximum lift coefficient was obtained from figure 6, and an increment in section lift coefficient resulting from a flap deflection of about 50° was estimated from data in references 1 and 2. The effect of half rated power on the maximum lift coefficient was obtained from data on tests of powered models of multiengine airplanes. This lift coefficient determined the landing speed.

The maximum level speed, maximum rate of climb, speed for best climb, and landing speed for the three loading conditions mentioned above and also the maximum range for three flying conditions are presented in table II. The values given are for sea-level performance.

Figure 21 seems to indicate that greater power would be required by the conventional-body airplane than by the lifting-body airplane at low speeds, but actually this would probably not be so. The model from which the drag coefficients for the conventional body were estimated had no fillets, and with the type of fuselage-wing juncture used, proper filleting would greatly reduce the drag, and hence the power required at low speeds. Thus, to be fair, the low-speed characteristics should not be compared

directly, and, therefore, the range, landing speed, and rate of climb should not be estimated for the conventional-body airplane from the power curves shown. However, at high speeds, where the filleting has little effect, the power curves for both types of cargo airplane are very closely similar, indicating that the fuselage shape in this case makes only a small difference in the performance.

Longitudinal stability and control.- The estimated longitudinal stability and control characteristics are summarized in the form of horizontal-tail area required for various cargo-body locations. The most critical requirements were for stability with the center of gravity in its most rearward position and for trim in the landing attitude with a fixed stabilizer with the center of gravity in its most forward position. The tail area required for any body-wing configuration and center-of-gravity range is shown in figure 23. The curves sloping downward to the right indicate the tail area required for power-off neutral stability; the curves sloping upward to the right indicate the tail area required to trim the airplane in the landing condition with the body on, fully loaded; the horizontal line indicates the tail area required to trim the airplane for landing with the cargo body off. The dotted lines have the same significance as the solid lines, except that they show the tail area required with all the centers of gravity in their normal positions. The normal centers of gravity are:

Airplane, body off	30 percent M.A.C.
Cargo body	35 percent body chord
Cargo	35 percent body chord

The center of gravity of the airplane with the body off was varied ±5 percent mean aerodynamic chord, and the cargo center of gravity was varied ±5, ±10, ±15, ±20, and ±25 percent mean aerodynamic chord from the normal position. The body-off center of gravity was considered to be in its maximum forward position when the cargo was forward, and vice versa.

With the body off, and for the center-of-gravity range chosen, the minimum tail area required to trim the airplane in landing is 18.8 percent of the wing area, the absolute minimum of tail area required for the airplane regardless of cargo center-of-gravity position or body

location. However, the restrictions imposed by the cargo center-of-gravity position or body location may require a larger minimum tail area. For example, suppose the maximum rearward cargo center-of-gravity shift is limited to 15 percent mean aerodynamic chord and the maximum forward shift to 20 percent mean aerodynamic chord. The body position at which the same tail area will be just sufficient for both stability and trim will be found at the point of intersection of the curves in figure 23 for the cargo center of gravity 15 percent behind and 20 percent ahead of the normal center of gravity. The minimum tail area required for this condition is 19.9 percent of the wing area, and the body location to meet these conditions is such that the body quarter-chord point is 9 percent mean aerodynamic chord ahead of the wing quarter-chord point. If the body is located farther ahead of the wing, a larger tail area will be required to trim the airplane for landing; this tail area will be more than sufficient to give neutral stability. If the maximum forward location of the cargo center of gravity in the above example is restricted to 10 percent ahead of the normal position, then the minimum tail area is governed by the requirements for landing with the body off, and will be independent of body location, as long as the body quarter-chord point is located between 12 and 16.5 percent mean aerodynamic chord ahead of the wing quarter-chord point.

The curves in figure 23, however, are generally applicable only to power-off flight, since the effects of power were neglected in the calculations on which the curves were based. The effects of power would be difficult to determine without making further tests. Probably, however, with power on, the tail area required for stability would be increased while the tail area required for trim would be decreased. Figure 23 shows that the effect on the minimum tail area required will depend on the relative magnitude of the stability and trim effects of power, but regardless of the relative magnitude of these effects, the body location that requires the smallest tail area will be further forward than indicated in figure 23.

In figure 24 is shown the variation of the center of gravity of the complete airplane with cargo-body location for different cargo center-of-gravity locations. The cargo-body location and center-of-gravity locations correspond to those shown in figure 23 on the curves which indicate the tail area required for neutral stability. Since the center-of-gravity location in a neutrally stable

airplane corresponds to the airplane's neutral point, the center of gravity of the airplane from figure 24 corresponding to any given cargo body and cargo location will give the neutral point corresponding to the horizontal tail area found in figure 23 from the same cargo body and cargo location. Thus, the power-off neutral point of the cargo airplane may be found by use of figures 23 and 24.

Once the neutral point is determined, the static margin for any center-of-gravity location may be ascertained by finding the distance between the neutral point and the center of gravity. Figure 24 may be used for finding the static margin for any of the conditions in the range covered by this figure. However, to be perfectly general for any combination of centers of gravity of the empty airplane and cargo load, the center of gravity of the complete airplane may be calculated by use of equation (A-5) in appendix A.

CONCLUDING REMARKS

The performance and longitudinal stability and control characteristics estimated in this report are only approximations, neglecting certain factors and making assumptions or estimations of others. However, a comparison of the polars obtained by the method of analysis used with experimental results obtained for a complete model of a specific airplane shows that the method will give reasonably good comparative performance estimates. Comparison of the power curves for the proposed design with those for a conventional airplane of the same size indicates no great difference in potential performance. The analysis also indicates that stability and control problems are no more difficult to solve than for other large airplanes. Therefore, no further investigation of the general aerodynamic characteristics of the lifting-body type of airplane is considered necessary; however, the usual wind-tunnel tests of a powered model of any specific design would still be desirable.

On the basis of the comparison made, any advantages which the lifting-body type of cargo airplane may have over the more conventional types are probably chiefly

dependent on nonaerodynamic factors, which were not considered in this report.

Langley Memorial Aeronautical Laboratory
National Advisory Committee for Aeronautics
Langley Field, Va.

APPENDIX A

PERFORMANCE CALCULATIONS

(All performance figures are at sea level.)

Drag.- The minimum profile drag was estimated by adding increments of drag coefficients due to wing, cargo body, booms, tail, and engine nacelles. The coefficients were all based on the total wing area, including that part within the booms and cargo body.

$$\text{Wing increment} = C_{D_{o_w}} \left(\frac{S - 500}{S}\right) = 0.00974$$

where $C_{D_{o_w}} = 0.0110$ (fig. 6.)

$S = 4375$ sq ft

500 is the wing area within the cargo body.

$$\text{Body and boom increment} = C_{D_{o_{c+b}}} \frac{S''}{S''_b} \frac{S_b}{S} = 0.00961$$

where $C_{D_{o_{c+b}}} = 0.0102$. (See appendix B and fig. 17.)

$S'' = 6$ sq ft

$S''_b = 1.888$ sq ft

$S_b = 1300$ sq ft

$$\text{Tail increment} = C_{D_{o_t}} \left(\frac{S_{t+s}}{S}\right) = 0.00259$$

$C_{D_{o_t}}$ is the minimum profile-drag coefficient of NACA 0009 = 0.0074 (reference 3).

$S_{t+s} = 35$ percent S.

$$\text{Engine nacelle increment} = C_{D_{o_n}} \frac{4S_n}{S} = 0.00134$$

$C_{D_{o_n}} = 0.092$ (reference 4).

$S_n = 15.9$ sq ft

Total minimum drag coefficient:

$$C_{D_o} = 0.00974 + 0.00961 + 0.00259 + 0.00134 = 0.0233$$

The minimum profile-drag coefficient for the Douglas C-74 was calculated in the same manner from data in figure 14 with the wing incidence at $2\frac{1}{2}^{\circ}$. These data are for tests of a fuselage representing the C-74, and the minimum profile drag is

$C_{D_o} = C_{D_{o_w}}$ + body increment + tail increment + engine nacelle increment = 0.0245

$C_{D_{o_w}} = 0.0110$

Body increment = $C_{D_{o_b}} \frac{S''}{S_m} = 0.00833$

$S'' = 6$ sq ft

S_m is the wing area which a scale model with the same body would have = 3.6 sq ft

Tail increment = $C_{D_{o_t}} \frac{S_t}{S} = 0.00286$

where the ratio of tail to wing area corresponds to that of the full-size airplane.

Nacelle increment = $C_{D_{o_n}} \frac{4S_n}{S} = 0.00234$

Lift-drag polars.- The estimated lift-drag polar for the Douglas C-74 is shown in figure 19. With it are shown experimental values of the lift and drag of a complete model of the C-74. These experimental data were obtained at approximately the same Reynolds number and turbulence factor as the present tests. The disagreement between the estimated and experimental polars at high lift coefficients results from the fact that the data in figure 14 were obtained from tests of a low-wing and circular-fuselage model without fillets at the wind-fuselage juncture, which leads to early separation and high drag at moderately high angles of attack. The agreement between the estimated and experimental values throughout most of the lift range indicates that the method used for obtaining the lift-drag polars is fairly good.

A lift-profile-drag polar was drawn approximately parallel to the polars in figure 7 for the wing 12-inch body-boom combination, but using the minimum drag coefficient estimates above. The induced drag of the wing, equal to $\frac{C_L^2}{\pi A}$, was added to the values of drag obtained from this polar where C_L is the lift coefficient corresponding to the profile-drag coefficient on the polar, and A is the wing aspect ratio of 9.15.

In figure 20, the complete airplane lift-drag polar is shown, and with it are compared the polars for the cargo airplane with the body off, and with the body replaced by drag equivalent to flat plates of 50 and 100 square feet.

In order to make the comparison between the lifting body and the conventional body directly, the drag was estimated for an airplane with a body the shape of that of the C-74 but with a cargo space, gross weight, and wing area the same as that of the lifting-body airplane being considered. The calculations were made in the same manner as above, and the minimum profile-drag coefficient was estimated to be 0.0217. Using the lift-profile-drag polar from figure 14 as before and adding the wing induced drag, the value of minimum drag coefficient was found to be 0.0223, and the complete polar is shown in figure 20.

Power curves.- The horsepower required was calculated from the relationship:

$$hp_r = \frac{C_D(S\rho/2)V^3}{550} \qquad (A\text{-}1)$$

where C_D drag coefficient at a given lift coefficient

$S = 4375$ sq ft

$\rho = 0.002378$ slug/cu ft

V = airspeed, ft/sec; calculated from the given lift coefficient for wing loadings of 40 lb/sq ft for the fully loaded airplane, 25 lb/sq ft for the lightly loaded airplane, and 20 lb/sq ft for the airplane with the body off.

The horsepower-available curve was prepared from an engine-propeller characteristic chart for full rated power (8800 hp). The power curves are shown in figure 21.

Performance.- The maximum speed occurs where the required horsepower is equal to the available horsepower, that is, where the power curves intersect. The speed for the best climb occurs at the speed where the difference between the horsepower available and the horsepower required is greatest, and can be found from the power curves where the difference in ordinates is greatest. To find the maximum rate of climb, the maximum excess horsepower is multiplied by 550 to get foot-pound per second units of power and divided by the weight of the airplane to get the rate of climb in feet per second.

The range was calculated at the maximum lift-drag ratio and at two values of constant brake horsepower, the minimum brake horsepower required for the fully loaded airplane and an arbitrary value of 6000 brake horsepower. The minimum brake horsepower required (4760 bhp) was obtained from figure 21 by dividing the minimum value of the horsepower-required curve by the engine-propeller efficiency. In figure 22 is shown the maximum range that the airplane can be flown with any weight of cargo, assuming an initial gross weight of 175,000 pounds.

The range at constant lift-drag ratio was calculated from the following equation:

$$R = 375 \frac{\eta}{f} \frac{L}{D} \log_e \frac{W}{W - W_f} \qquad (A-2)$$

where L/D is the maximum lift-drag ratio obtained from figure 19, $\eta = 0.84$, $f = 0.47$

At constant power, the range was calculated from the equation

$$R = \frac{W_f \times V}{f \times hp} \qquad (A-3)$$

where V is an average between the full loaded and empty speeds for the given horsepower (fig. 20)

$f = 0.46$ at 4760 bhp

0.53 at 6000 bhp

Landing speed.- The maximum lift coefficient of 1.35 was obtained from figure 6, and the increment in section lift coefficient of 1.15 caused by the flaps was estimated from references 1 and 2. The assumption was made that landings would be made with half rated power, and the effects of power on the maximum lift coefficients obtainable were estimated from data on tests of several powered wind-tunnel models. It was assumed that the effect of propeller operation was to increase the dynamic pressure over that part of the wing immersed in the slipstream. The data used for the specific calculations were taken from the afore-mentioned tests of the Douglas C-74 since the C-74 used the same type of engine and is almost as large as the cargo airplane considered in this report. The effective increase in dynamic pressure in the slipstream was calculated as follows:

At a given angle of attack, the difference between the lift coefficients with the power off and the lift coefficients with power on was measured for several model configurations. Assuming that the additional lift with the power on came only from that part of the wing immersed in the slipstream and that the power-off lift coefficient was uniform across the span (since the model had full-span flaps), the measured lift coefficient increment was divided by the fraction of the wing area immersed in the slipstream and added to the power-off lift coefficient and this sum was divided by the power-off lift coefficient to get the ratio of dynamic pressure in the slipstream to the free-stream dynamic pressure, which proved to be 5/3. The process was then reversed to get the lift coefficient of the part of the cargo airplane wing immersed in the slipstream. The maximum lift coefficient was then obtained by adding the lift as follows:

$$C_L = C_{L_1} \frac{S_1}{S} + C_{L_2} \frac{S_2}{S} + \frac{5}{3} C_{L_2} \frac{S_3}{S}$$

where C_{L_1} is the maximum section lift coefficient without flaps = 1.35, and C_{L_2} is the maximum section lift coefficient with flaps deflected = 2.50

$$\frac{S_1}{S} = 0.429$$

$$\frac{S_2}{S} = 0.206$$

$\frac{S_3}{S} = 0.365$

The additional lift due to the cargo body was not considered, since it was assumed that this would be nullified by the negative lift required for trim.

This gives a maximum lift coefficient of 2.62. The landing speed in miles per hour is given by

$$V = \sqrt{\frac{391W}{C_L S}}$$

where $\frac{W}{S}$ is the wing loading.

For wing loadings of 40 pounds per square foot (full load), 25 pounds per square foot (light load, body on), and 20 pounds per square foot (light load, body off), the landing speeds are 78, 61, and 55 miles per hour, respectively.

The setting of the wing relative to the body was chosen to give a uniform spanwise lift distribution in the vicinity of the cargo body at a cruising lift coefficient of 0.75 to secure as high a lift-drag ratio as possible. This setting was obtained as follows:

$$\frac{0.75}{C_{L_{a_w}}} = \alpha_w$$

$$\frac{c_w}{c_b}\frac{0.75}{C_{L_{a_b}}} = \alpha_b$$

$i_w = \alpha_w - \alpha_b$ = angle between the zero-lift lines of wing and body. $C_{L_\alpha} = 0.0828$ for wing and 0.040 for body. The wing incidence was estimated to be 3°.

STABILITY AND CONTROL CALCULATIONS

In the stability and control analysis, the geometric configurations previously described and the maximum cargo

load of 40 percent of the gross weight were assumed. In addition, the following approximations and assumptions were made:

The effects of power were neglected.

The effect of the vertical location of the center of gravity was neglected.

C_{L_α} of the wing and tail were 0.0828 and 0.0720, respectively, taken from section data (reference 3) and corrected for the assumed aspect ratio. The ground effect on these lift-curve slopes was small and, therefore, neglected.

$C_{L_{\alpha_b}} = 0.04$. The basis for this assumption is given in appendix B.

The aerodynamic centers of the wing, body, and tail were considered to be at their respective quarter-chord points.

$$C_{m_o} = -0.076$$

$$C_{m_{o_b}} = -0.100$$

$$C_{m_{o_t}} = 0$$

$$q_t/q = 0.9$$

$\frac{\partial \epsilon}{\partial \alpha}$ is 0.5 in free air and 0.15 near the ground.

The reduction in downwash near the ground was estimated from reference 5. The value of 0.5 in free air was obtained from an analysis of pitching-moment data for an airplane of similar configuration. It was assumed that the trailing vortices shed by the cargo body would cause a downwash over the central portion of the tail and an upwash over the part of the tail outside the booms, so that the average effective downwash on the tail would be unaffected by the presence or absence of the cargo body.

References 6 and 7 indicate an elevator effectiveness of 0.7 for the tail configuration used. Data from tests

of a tail configuration similar to that of the airplane under consideration were used to find the maximum tail lift coefficient for the landing condition. Estimating the angle of attack of the tail by:

$$\alpha_t = \left[\alpha\left(1 - \frac{\partial \epsilon}{\partial \alpha}\right) - \Delta\alpha_f \left(\frac{\partial \epsilon}{\partial \alpha}\right) + i_t\right] \qquad (A\text{-}4)$$

and using a maximum elevator deflection of -25°, the lift coefficient of the tail was estimated at -0.5.

The tail setting i_t was assumed to be fixed, and to be set for trim with zero elevator deflection at a cruising lift coefficient of 0.75 with the centers of gravity in their normal locations. This tail setting will vary with body location and tail area, but an average value of about -7° was used. This corresponds to a setting of about -3° with respect to the wing chord line.

Full flap deflection of 50° was assumed for the landing condition. The center of pressure of the flap lift was assumed to be at 0.55c. At full deflection, a section lift coefficient increment due to the flaps was estimated from references 1 and 2 to be 1.15, which gives a value of 0.65 for C_{L_f} based on the total wing area.

$\alpha = 16^\circ$ for the landing condition

S = 4375 sq ft, S' = 3875 sq ft since 500 sq ft of wing area is within the cargo body

$$k = \frac{S}{S'} = 1.129$$

$$\frac{S_b}{S'} = 0.3355$$

$$\frac{c_b}{c} = 2.97$$

$$i_w = 3^\circ$$

$$\frac{z_b}{c} = 0.297$$

The center-of-gravity position varies with the cargo-body location according to the following relationship:

$$\frac{x}{c} = 0.1\left(5\frac{x_e}{c} + \frac{z_b}{c} + 4\frac{z_c}{c} - 5\frac{a}{c}\right) \qquad (A\text{-}5)$$

where $\frac{z_b - z_c}{c}$ is the location of the cargo ahead of its normal position. The neutral point was calculated from the following relationship:

$$\frac{x_n}{c} = \frac{\left[\left(1 - \frac{\partial\epsilon}{\partial\alpha}\right)\frac{q_t}{q}\frac{S_t}{S'}\frac{l}{c}C_{L_{\alpha_t}} - \frac{S_b}{S'}\frac{a}{c}C_{L_{\alpha_b}}\right]}{\left[C_{L_\alpha} + \frac{S_b}{S'}C_{L_{\alpha_b}} + \left(1 - \frac{\partial\epsilon}{\partial\alpha}\right)\frac{q_t}{q}\frac{S_t}{S'}C_{L_{\alpha_t}}\right]} \qquad (A\text{-}6)$$

S' is used for calculations with the body on, and S is used instead of S' with the body off.

The tail area required for stability is that area which makes $x_n = x$ for a given cargo-body location.

To get the tail area required to trim the airplane in the landing condition, the following relationship was used:

$$k\frac{S_t}{S} = \frac{\frac{S_b}{S'}\frac{c_b}{c}C_{m_{o_b}} + C_{m_o} + \alpha C_{L_\alpha}\frac{x}{c} + k C_{L_f}\left(\frac{x}{c} - 0.3\right) + \left(\alpha - i_w\right)\frac{S_b}{S'}C_{L_{\alpha_b}}\frac{(a+x)}{c}}{C_{L_t}\frac{q_t}{q}\frac{l-x}{c}} \qquad (A\text{-}7)$$

k was used for calculations with body on, and was not used with body off.

APPENDIX B

The drag data from the tests were broken up into several components and plotted in figure 17 for analysis.

The cargo-body drag increment, when extrapolated to zero body width, was not zero. The drag increment at zero body width coincided with the calculated skin friction of the sides, as indicated in the discussion of the test data. The minimum profile drag of the cargo body was estimated from figures 91 and 92 of reference 3 and this value was used to calculate the drag of the wing-body combination with different body widths according to the relation:

$$C_{D_o} = \frac{C_{D_{o_w}} S' + C_{D_{o_b}} S_b}{S}$$

The variation of this drag plus the skin friction of the sides with body width compared with the measured value of the drag of the wing-body combination is shown in figure 17. There is a discrepancy of about 0.0028 between the measured and calculated values of minimum drag coefficient at the largest body width. However, tuft tests made on the model showed bad flow breakaway around the fairly blunt trailing edge of the body, even at negative angles of attack. The trailing-edge angle of the body section used was about 50°, and additional tests were made with the trailing edge of the body extended to form an angle of about 30°. Tuft tests indicated that the flow was greatly improved, and force tests showed a decrease in minimum drag coefficient of 0.0030. (See fig. 16.) These additional tests were made with the wing 22-inch body-boom combination and the measured value of the drag is shown in figure 17. When the decrease in drag of this combination is subtracted from the measured drag of the wing-body combination, the agreement between the measured and calculated drag is good. The difference in drag coefficient is 0.0002, which is less then the experimental error involved.

It was assumed that the reduction in drag caused by extending the trailing edge of the body was due to the reduction of the trailing-edge angle to 30°. Since the NACA four-digit series airfoils of 25 percent thickness have a trailing-edge angle of about 30°, a section of this type was chosen for the cargo-body configuration.

Another consideration involved in choosing the section was that it had to enclose the wing plus a cargo space about 10 feet high and 40 feet long. The NACA 6325 section met these conditions, but this section had to be modified by reflexing the trailing edge from the 60 percent chord point back to allow ground clearance for the body and booms during landing. This modification did not affect the trailing-edge angle or the cargo space. Regardless of the spacing of the booms, the increment of drag added to the wing by the booms is shown to be constant. (See fig. 10.) The skin-friction drag of the booms was calculated at a Reynolds number based on the test velocity and boom length, assuming a turbulent boundary layer along the boom. The total drag coefficient increment of the two booms was 0.0078, while the calculated skin-friction increment was 0.0063, or about 81 percent of the total boom drag. The rest was form and interference drag.

The drag of the wing-body-boom combination, from figure 7, was just the simple sum of the drags of the three components. The difference between the drag of this combination and of the wing-body combination is constant and equal to the increment of drag of the booms on the wing alone. This indicates that the interference between the body and the booms was equal to the skin friction of the sides of the body and the part of the booms not exposed to the air stream.

The value of the cargo body-boom drag used in the performance calculations in appendix A was obtained as follows:

The skin friction of booms similar to those shown in figure 18 was calculated at a Reynolds number corresponding to the test conditions. To this was added the form drag and wing-boom interference, which were assumed to be the same as for the large booms used in the tests. The interference between the booms and body was assumed to be reduced by an amount equal to the skin friction on the body sides, and so the calculated drag of a cargo body of the same span-chord ratio as that used in the cargo airplane analysis, not including the skin friction of the sides, was added to the boom drag. This drag coefficient increment of the cargo body-boom combination is shown in figure 17, and its value is 0.0102.

The slope of the lift curve of the cargo body is of great interest in all the calculations. Therefore, the

value of this slope was estimated from the data of figures 6 and 9 and checked from simple theoretical considerations.

The experimentally estimated slope was obtained by subtracting the lift of the part of the wing not covered by the body from the lift of the wing-body combination at the same angle of attack and getting the resultant body lift coefficient based on the body area. The lift coefficient of the body was then plotted against the angle of attack and the slope measured. The method of getting the lift, by subtracting one large value from another to get a small increment, is not very accurate; therefore, the data obtained did not give a very smooth curve. The average slope for the 12-inch body was between 0.045 and 0.050.

The slope was then caclulated by replacing the wing and the body with two simple, superimposed horseshoe vortices, one representing the wing, and the other representing the body.

The angles of attack induced by the vortices on the wing and on the body are given by:

$$\alpha_{i_w} = \frac{(L/b)_w}{\pi q b_w} \qquad \text{(B-1)}$$

$$\alpha_{i_b} = \frac{(L/b)_b - (L/b)_w}{\pi q b_b} \qquad \text{(B-2)}$$

The angle of attack of the wing and body are given by:

$$\alpha_w = \alpha_{o_w} + \alpha_{i_w} \qquad \text{(B-3)}$$

$$\alpha_b = \alpha_{o_b} + \alpha_{i_w} + \alpha_{i_b} \qquad \text{(B-4)}$$

Assuming for the sake of simplicity that the wing is at zero incidence. and that the angle of attack of the wing is not affected by the body vortex since the body span is small compared to the wing span, then $\alpha_w = \alpha_b$

and

$$\alpha_{o_w} = \alpha_{o_b} + \alpha_{i_b} \qquad \text{(B-5)}$$

substituting for α_{i_b} from (B-2)

$$\alpha_{o_w} = \alpha_{o_b} + \frac{(L/b)_b - (L/b)_w}{\pi q b_b} \tag{B-6}$$

assuming that the section lift-curve slopes of both wing and body are equal to 2π per radian,

$$\frac{(L/b)_b}{\alpha_{o_b}} = \frac{c_b}{c_w}\frac{(L/b)_w}{\alpha_{o_w}} \tag{B-7}$$

combining (B-6) and (B-7),

$$\alpha_{o_w} = \alpha_{o_b} + \frac{(L/b)_w}{\pi q b_b}\left(\frac{\alpha_{o_b}\frac{c_b}{c_w} - \alpha_{o_w}}{\alpha_{o_w}}\right) \tag{B-8}$$

but

$$\frac{(L/b)_w}{\alpha_{o_w}} = C_{L_{\alpha_{o_w}}} qc_w = 2\pi q c_w \tag{B-9}$$

then combining (B-8) and (B-9),

$$\alpha_{o_w} = \alpha_{o_b} + \frac{2c_w}{b_b}\left(\alpha_{o_b}\frac{c_b}{c_w} - \alpha_{o_w}\right)$$

$$\alpha_{o_w}\left(1 + \frac{2c_w}{b_b}\right) = \alpha_{o_b}\left(1 + \frac{2c_b}{b_b}\right)$$

$$\frac{\alpha_{o_b}}{\alpha_{o_w}} = \frac{1 + \frac{2c_w}{b_b}}{1 + \frac{2c_b}{b_b}} \tag{B-10}$$

Now

$$\frac{C_{L_{\alpha_b}}}{C_{L_{\alpha_w}}} = \frac{\frac{\alpha_{o_b}}{\alpha} C_{L_{\alpha_{o_b}}}}{\frac{\alpha_{o_w}}{\alpha} C_{L_{\alpha_{o_w}}}}$$

but since $c_{l_{\alpha_{o_b}}} = c_{l_{\alpha_{o_w}}}$

$$\frac{C_{L_{\alpha_b}}}{C_{L_{\alpha_w}}} = \frac{a_{o_b}}{a_{o_w}} \qquad \text{(B-11)}$$

Therefore, combining (B-10) and (B-11),

$$C_{L_{\alpha_b}} = C_{L_{\alpha_w}} \frac{1 + \frac{2c_w}{b_b}}{1 + \frac{2c_b}{b_b}} \qquad \text{(B-12)}$$

For the test conditions with the 12-inch body,

$$C_{L_{\alpha_b}} = 0.096 \frac{1 + \frac{2 \times 12}{12}}{1 + \frac{2 \times 30.2}{12}} = 0.0477 \text{ per degree}$$

which checks very well with the experimental value estimated from figure 12. The corresponding value for the full-scale airplane configuration is $C_{L_{\alpha_b}} = 0.0352$. The value used in the analysis was slightly higher, since it was assumed that the booms would increase this value slightly.

As an additional check, the angle of zero lift of the wing-body combinations tested was calculated and compared with the measured values.

$$a_{L_o} = \frac{a_{L_{o_b}} C_{L_{\alpha_b}} S_b + a_{L_{o_w}} C_{L_{\alpha_w}} S_w}{C_{L_{\alpha_b}} S_b + C_{L_{\alpha_w}} S_w} \qquad \text{(B-13)}$$

where $a_{L_{o_b}}$ is the angle of zero lift of a conventional NACA section having approximately the same thickness and mean camber line as the cargo-body section, $= -2.0^\circ$.

$a_{L_{o_w}}$ is the wing angle of zero lift from figure 6, $= -4.1^\circ$.

$C_{L_{\alpha_b}}$ is the value calculated for each body width.

The comparison between measured and calculated values of the zero lift angle is shown in table III.

REFERENCES

1. Wenzinger, Carl J., and Harris, Thomas A.: Wind-Tunnel Investigation of an N.A.C.A. 23012 Airfoil with Various Arrangements of Slotted Flaps. NACA Rep. No. 664, 1939.

2. Wenzinger, Carl J., and Harris, Thomas A.: Wind-Tunnel Investigation of an N.A.C.A. 23021 Airfoil with Various Arrangements of Slotted Flaps. NACA Rep. No. 677, 1939.

3. Jacobs, Eastman N., Ward, Kenneth E., and Pinkerton, Robert M.: The Characteristics of 78 Related Airfoil Sections from Tests in the Variable-Density Wind Tunnel. NACA Rep. No. 460, 1933.

4. Wood, Donald H.: Tests of Nacelle-Propeller Combinations in Various Positions with Reference to Wings. III - Clark Y Wing - Various Radial-Engine Cowlings - Tractor Propeller. NACA Rep. No. 462, 1933.

5. Katzoff, S., and Sweberg, Harold H.: Ground Effect on Downwash Angles and Wake Location. NACA Rep. No. 738, 1943.

6. Silverstein, Abe, and Katzoff, S.: Aerodynamic Characteristics of Horizontal Tail Surfaces. NACA Rep. No. 688, 1940.

7. Ames, Milton B. Jr., and Sears, Richard I.: Determination of Control-Surface Characteristics from NACA Plain-Flap and Tab Data. NACA Rep. No. 721, 1941.

TABLE I

Specifications of proposed cargo airplane design:

Weights	Pounds	Percent of gross
Empty airplane with no cargo body	80,000	45.71
Cargo body	17,500	10
Cargo and/or fuel	70,000	40
Crew, oil, and fuel (minimum)	7,500	4.29
Gross	175,000	100.00

Wing	
Area (including area covered by body), sq ft	4375
Span, ft	200
Aspect ratio	9.15
Mean aerodynamic chord, ft	21.9
Airfoil section	NACA 4318
Incidence (between wing chord line and body chord line)	2°
Wing flaps	
Type	slotted
Chord	25 percent wing chord
Span	50 percent wing span
Angular deflection	50° down max.
Body	
Area, sq ft	1300
Span, ft	20
Chord, ft	65
Section	NACA 6325 (modified)
Cargo space, ft (approximately)	40 by 20 by 10

Horizontal tail (original design)		
Area	900 sq ft	20.6 percent wing area
Span, ft	64	
Chord, ft	15	
Aspect ratio	4.6	
Airfoil section	NACA 0009	
Elevator area	390 sq ft	43.5 percent tail area
Tail length (from c/4 of wing to c/4 of tail)	70 ft	320 percent M.A.C.

TABLE I - Concluded

Engines	
Type	Wright R-3350
Number	4
Take-off horsepower	2300
Normal rated horsepower	2200 at 2500 ft
Propellers	
Number of blades	4
Diameter, ft	16
Normal centers of gravity	
Airplane center of gravity, body off.	at 30 percent M.A.C.
Center of gravity of cargo body	at 35 percent of body chord
Center of gravity of cargo	at 35 percent of body chord

NATIONAL ADVISORY
COMMITTEE FOR AERONAUTICS

TABLE II

Load condition	Maximum level speed (mph)	Maximum rate of climb (fpm)	Speed for best climb (mph)	Landing speed with 1/2 rate power (mph)	Maximum range at		
					[a]Max. L/D (17.1) (miles)	[b]Min. bph (4760) (miles)	[c]6000 bph (miles)
Body on, gross weight (175,000 lb)	209	637	142	78	6410	5400	4350
Body on, light load (110,000 lb)	216	1465	123	61			
Body off, light load (87,500 lb)	231	2060	125	55			

[a]At an average cruising speed of 135 miles per hour
[b]At an average cruising speed of 155 miles per hour
[c]At an average cruising speed of 180 miles per hour

NATIONAL ADVISORY
COMMITTEE FOR AERONAUTICS

MR No. L5E09a

TABLE III

Body width (in.)	Calculated α_{L_o} (deg)	Experimental α_{L_o} (deg)
4	-3.98	-4.0
12	-3.68	-3.7
22	-3.31	-3.35

NATIONAL ADVISORY
COMMITTEE FOR AERONAUTICS

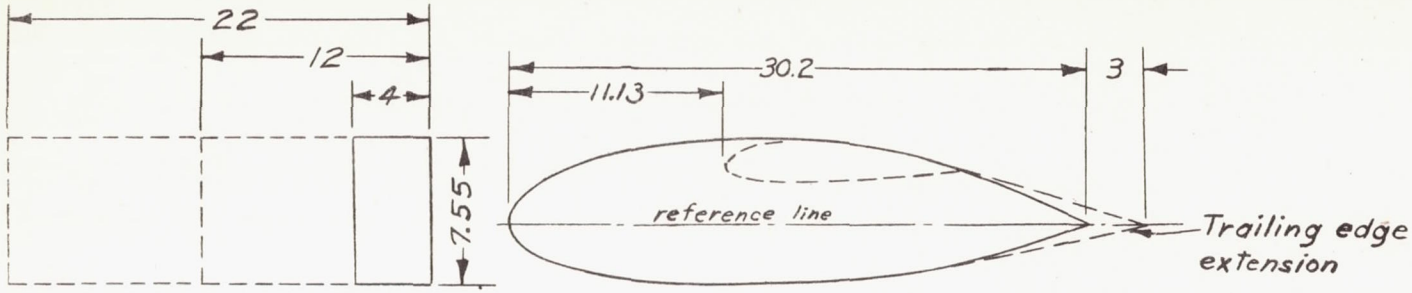

Ordinates of Cargo Body Profile.

Sta.	0	.377	.755	1.51	2.27	3.02	4.53	6.04	7.55	9.06	12.08	15.10	18.12	21.14	24.16	27.18	28.69	30.2
Upper	0	.98	1.39	1.97	2.41	2.75	3.29	3.71	4.01	4.22	4.37	4.28	4.01	3.44	2.62	1.50	.78	0
Lower	0	-.89	-1.24	-1.68	-2.01	-2.26	-2.60	-2.84	-3.01	-3.10	-3.17	-3.10	-2.89	-2.52	-1.96	-1.12	-.58	0

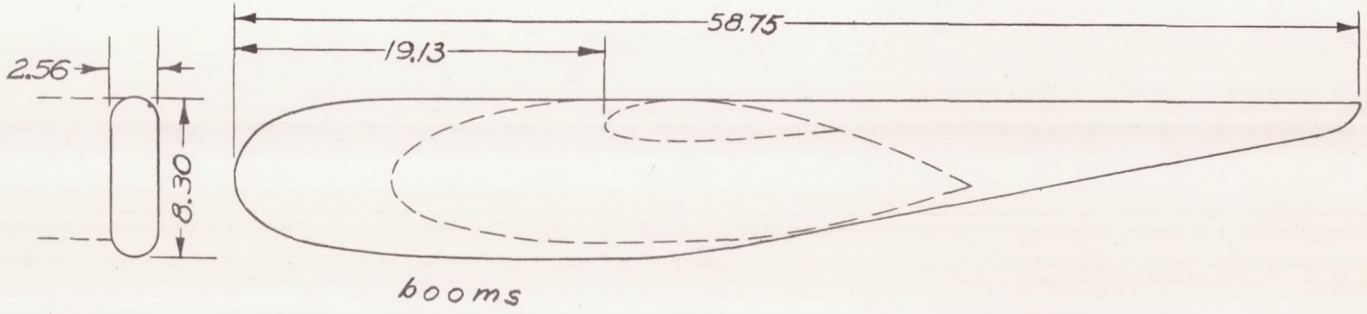

NATIONAL ADVISORY
COMMITTEE FOR AERONAUTICS

Figure 1.- Cargo-body and boom models.

MR No. L5E09a

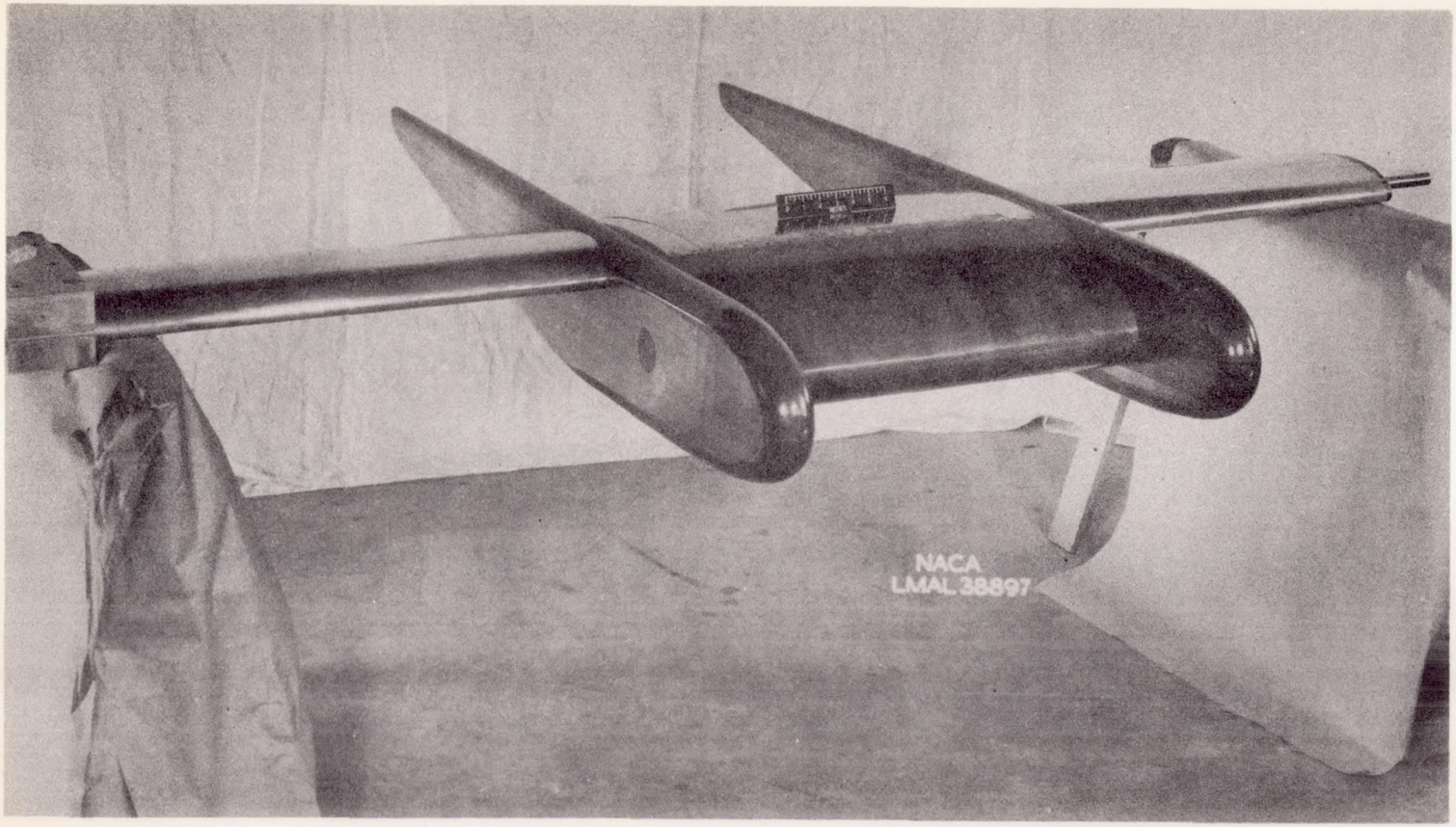

(a) Wing, 22-inch cargo body, and booms.

Figure 2.- Cargo body and boom configurations tested.

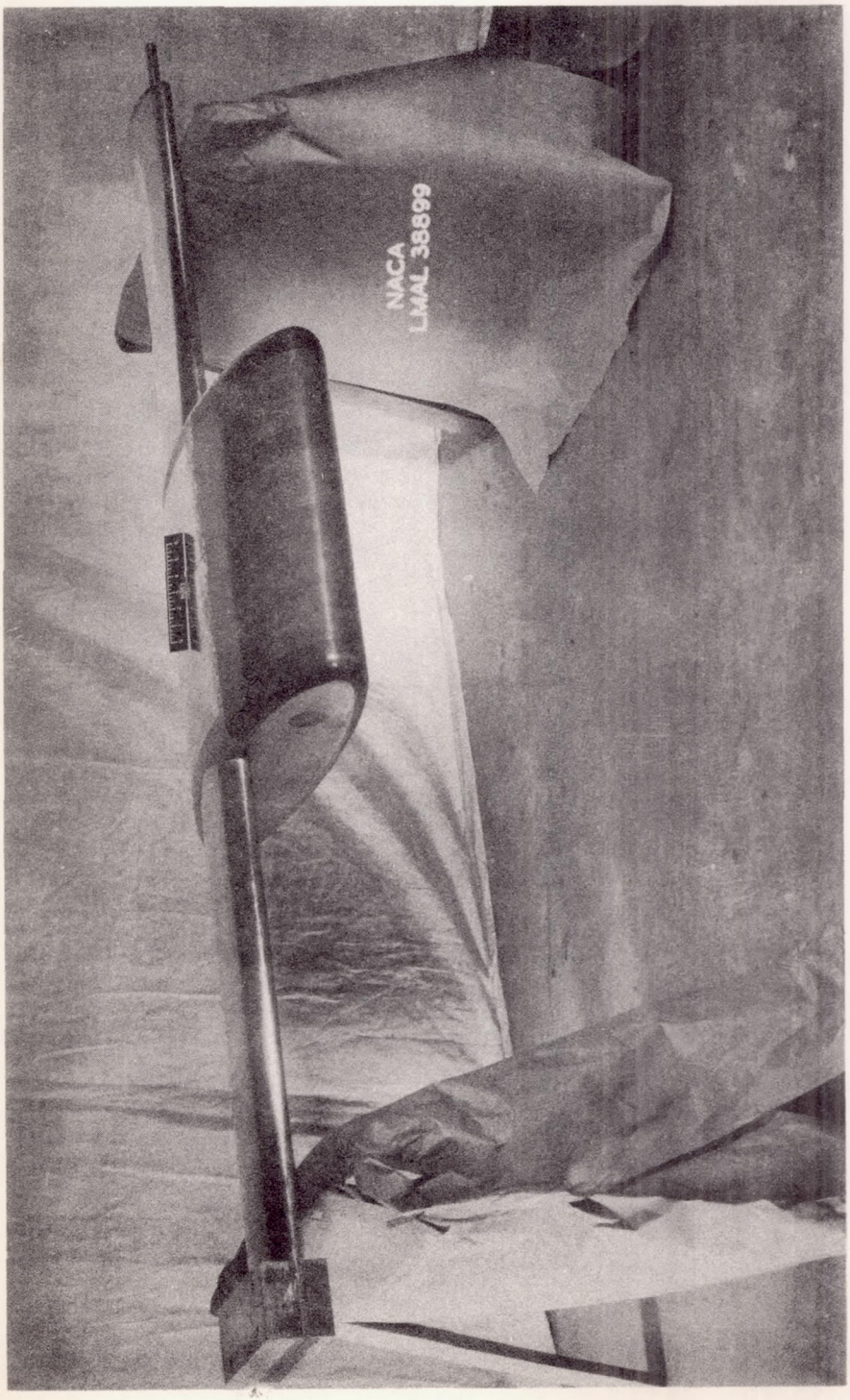

(b) Wing and 22-inch cargo body.

Figure 2.- Continued.

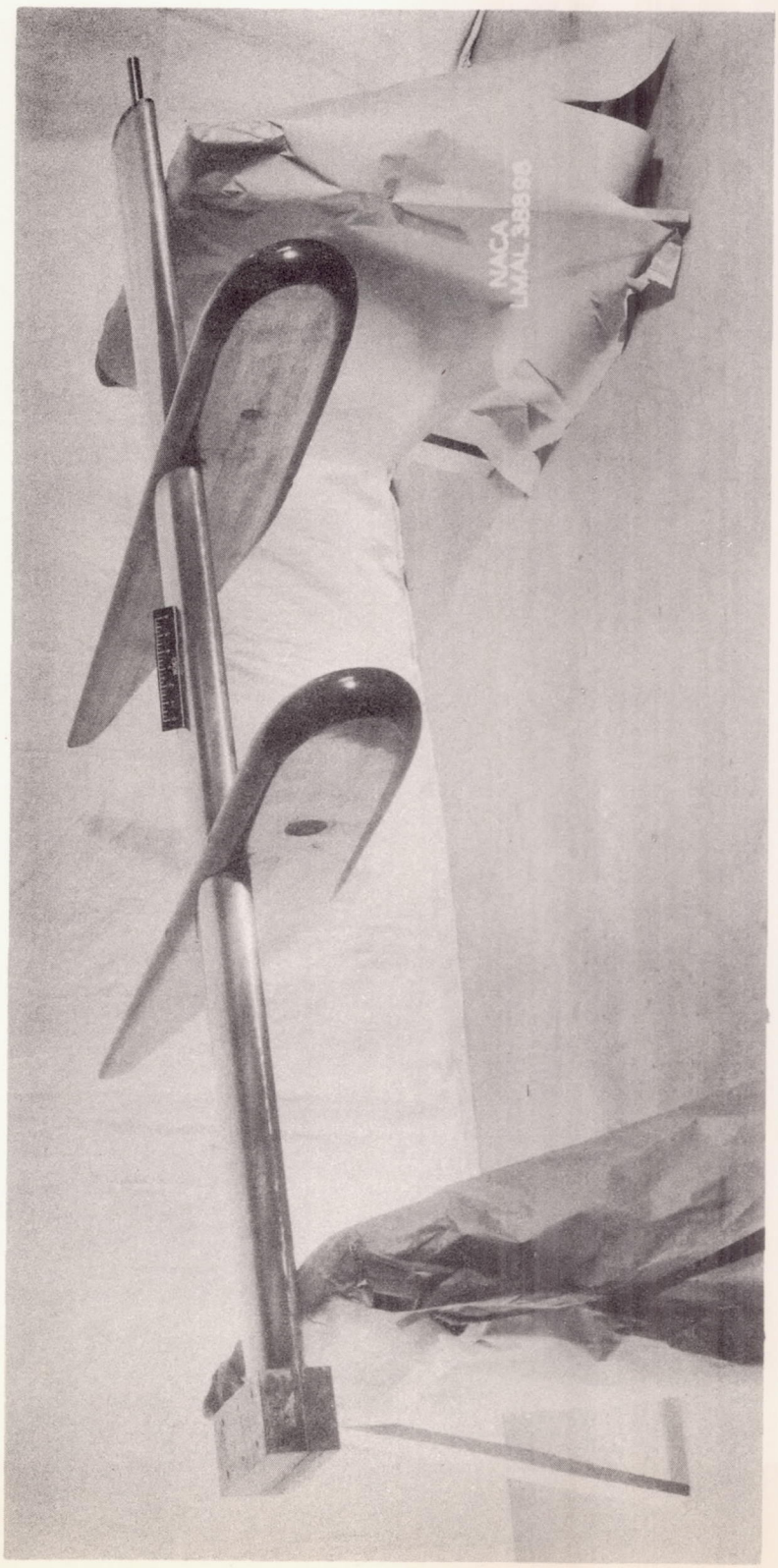

(c) Wing and booms.

Figure 2.- Continued.

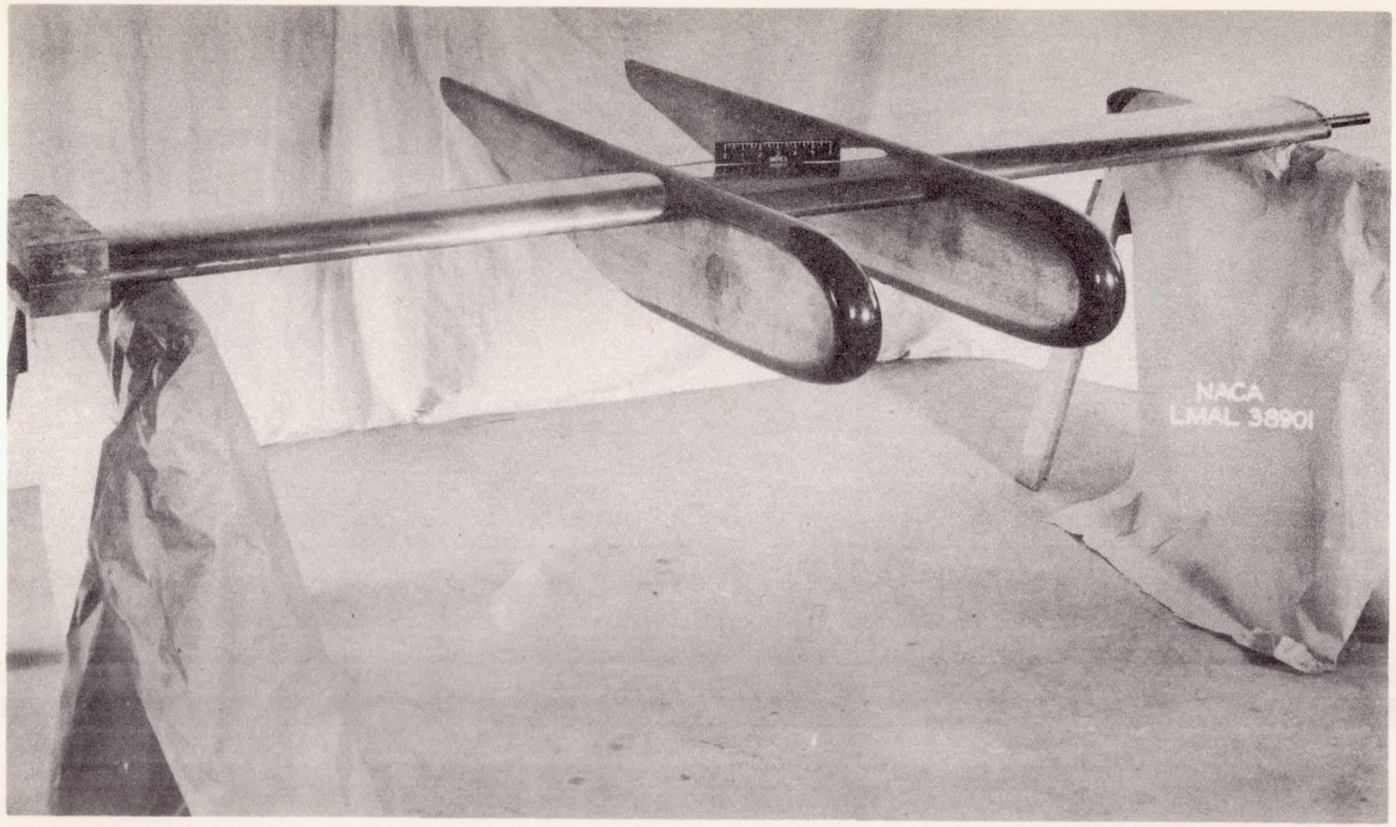

(d) Wing and booms, with increased chord wing between booms.

Figure 2.- Concluded.

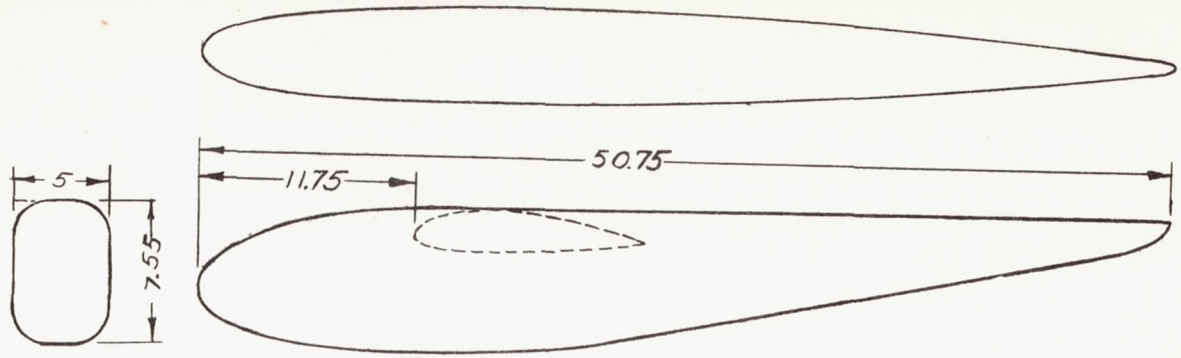

rectangular section body

NATIONAL ADVISORY
COMMITTEE FOR AERONAUTICS

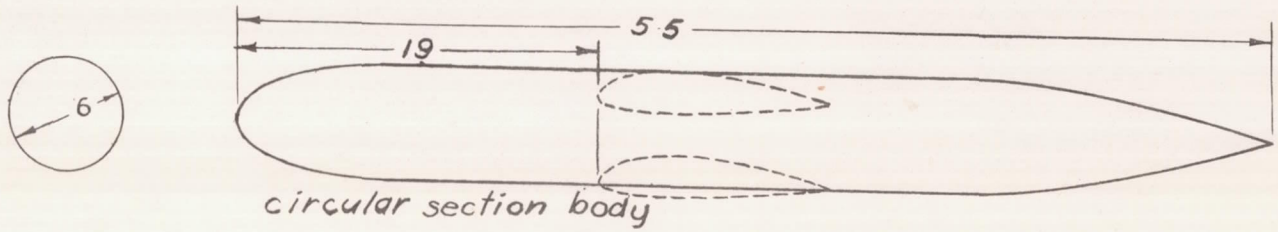

circular section body

Figure 3 - Conventional body models.

MR No. L5E09a

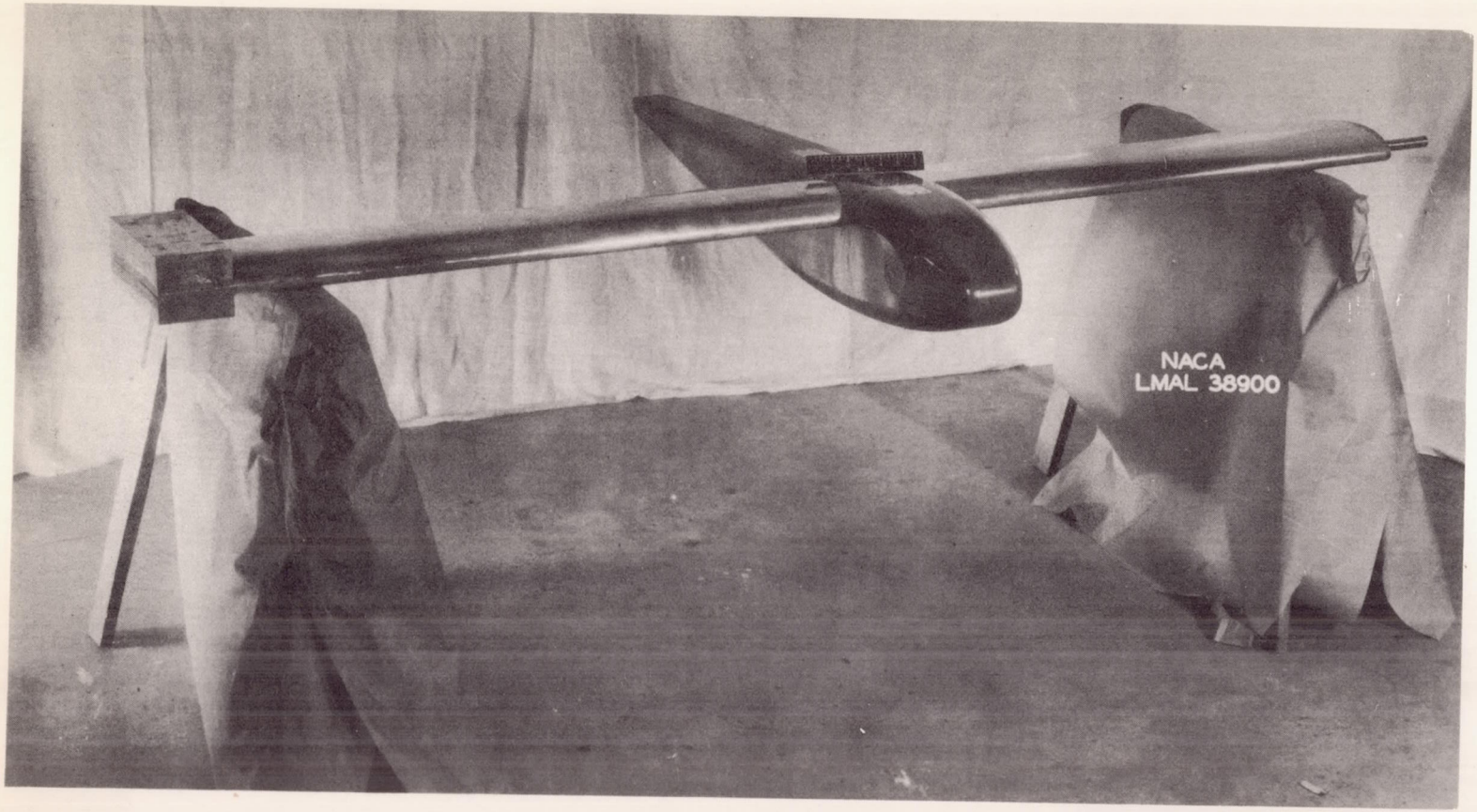

(a) Conventional rectangular body.

Figure 4.- Conventional body configurations tested.

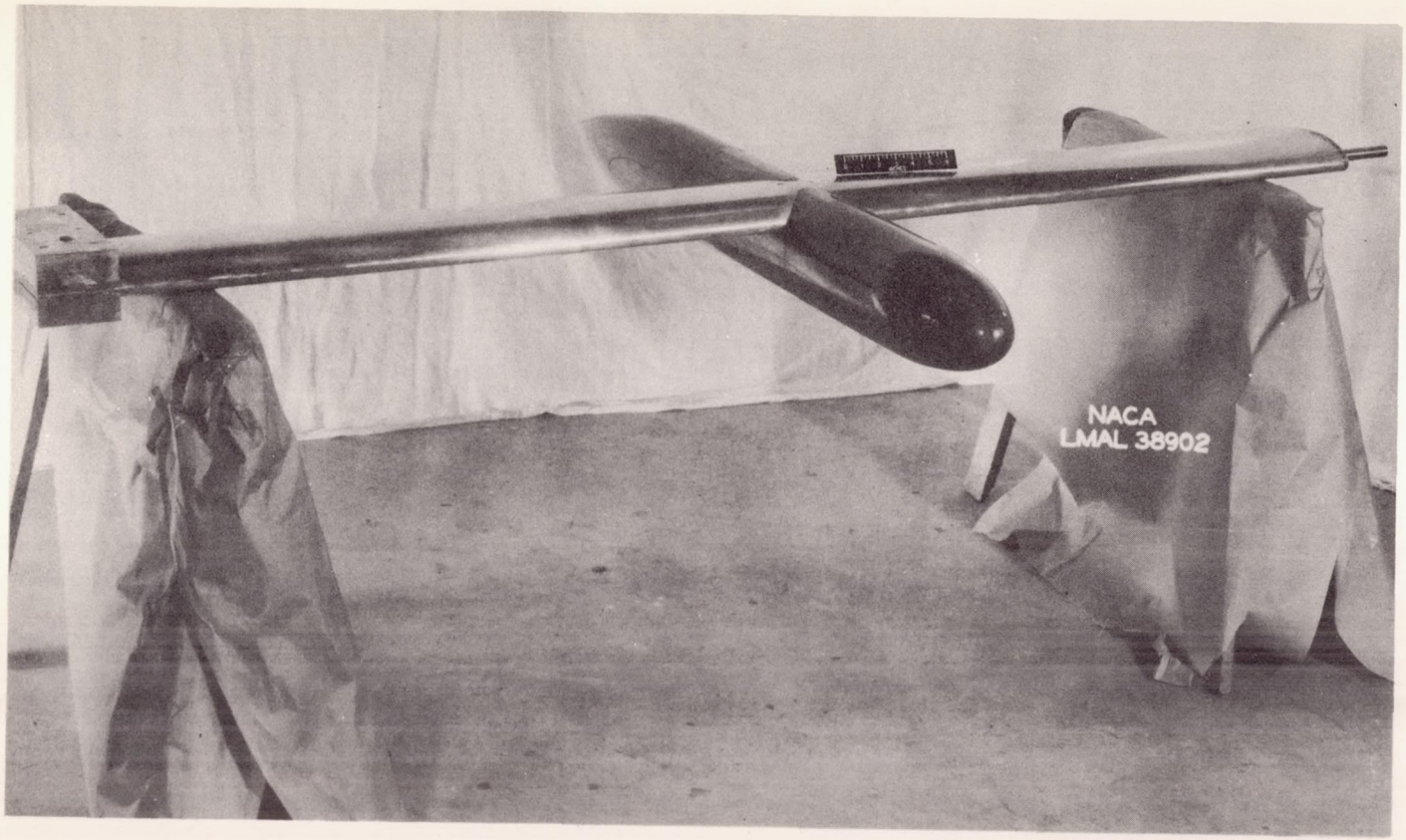

(b) High wing and circular body.

Figure 4.- Continued.

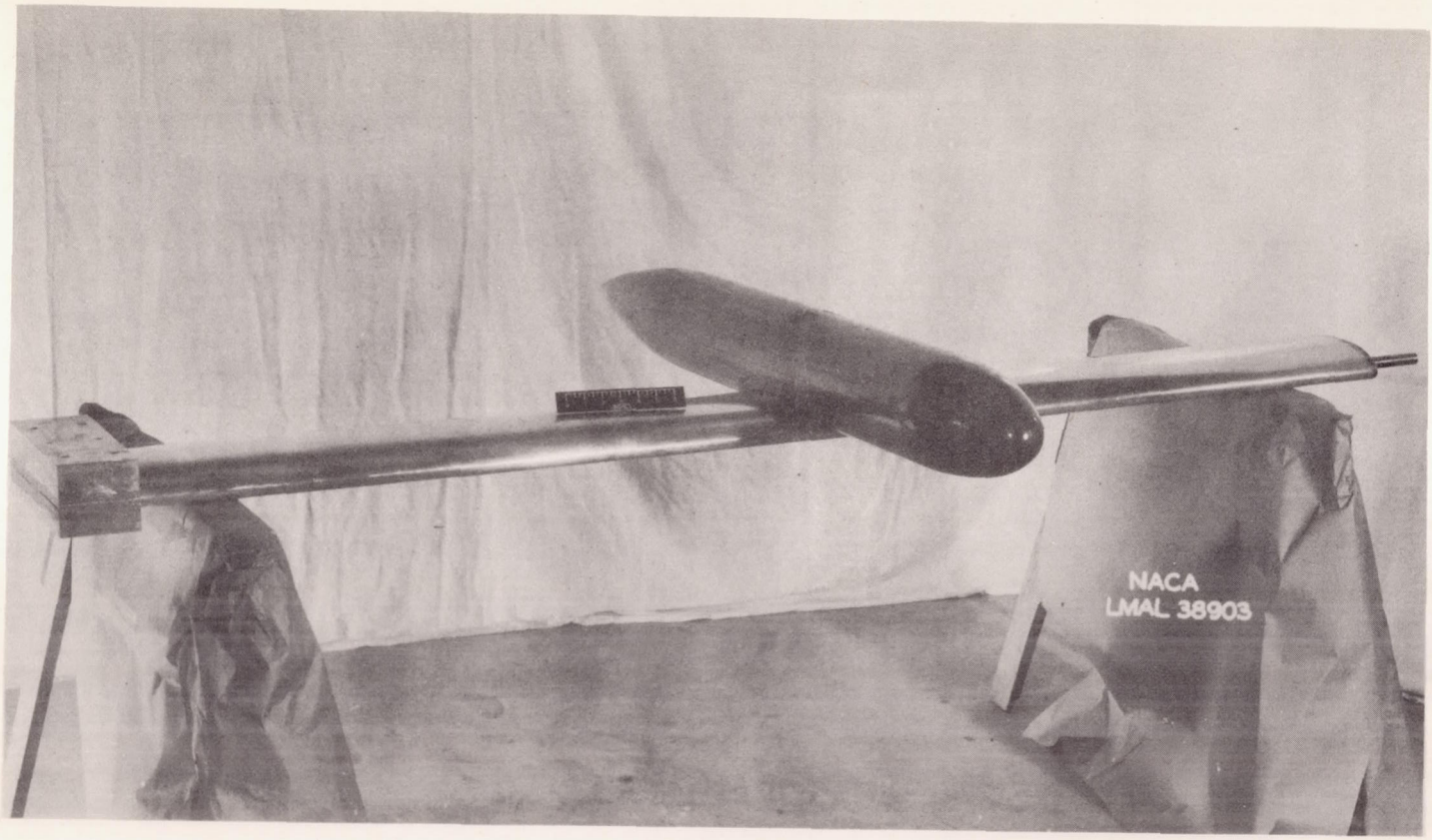

(c) Low wing and circular body.

Figure 4.- Concluded.

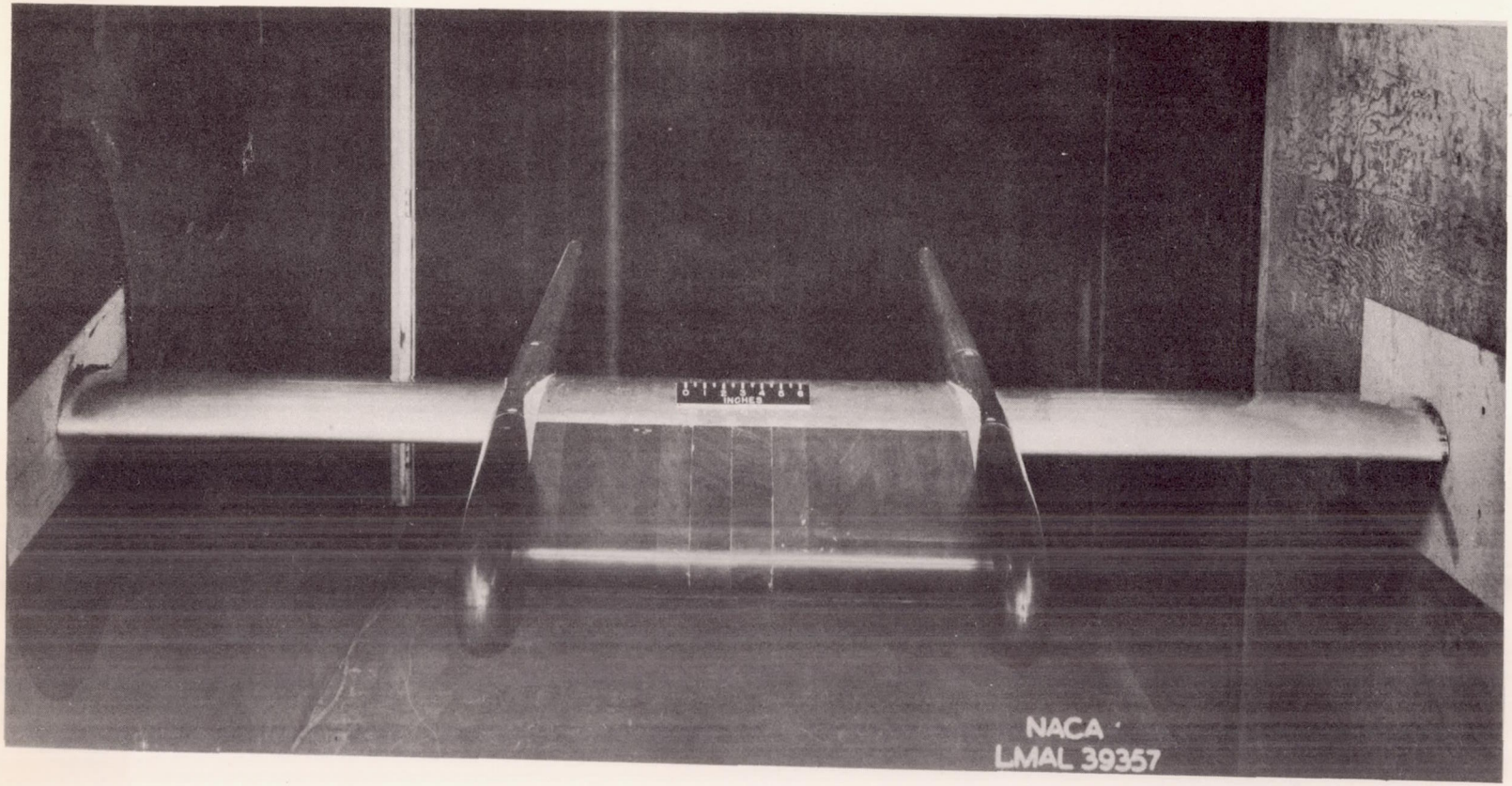

(a) Front view.

Figure 5.- Cargo model mounted in wind tunnel.

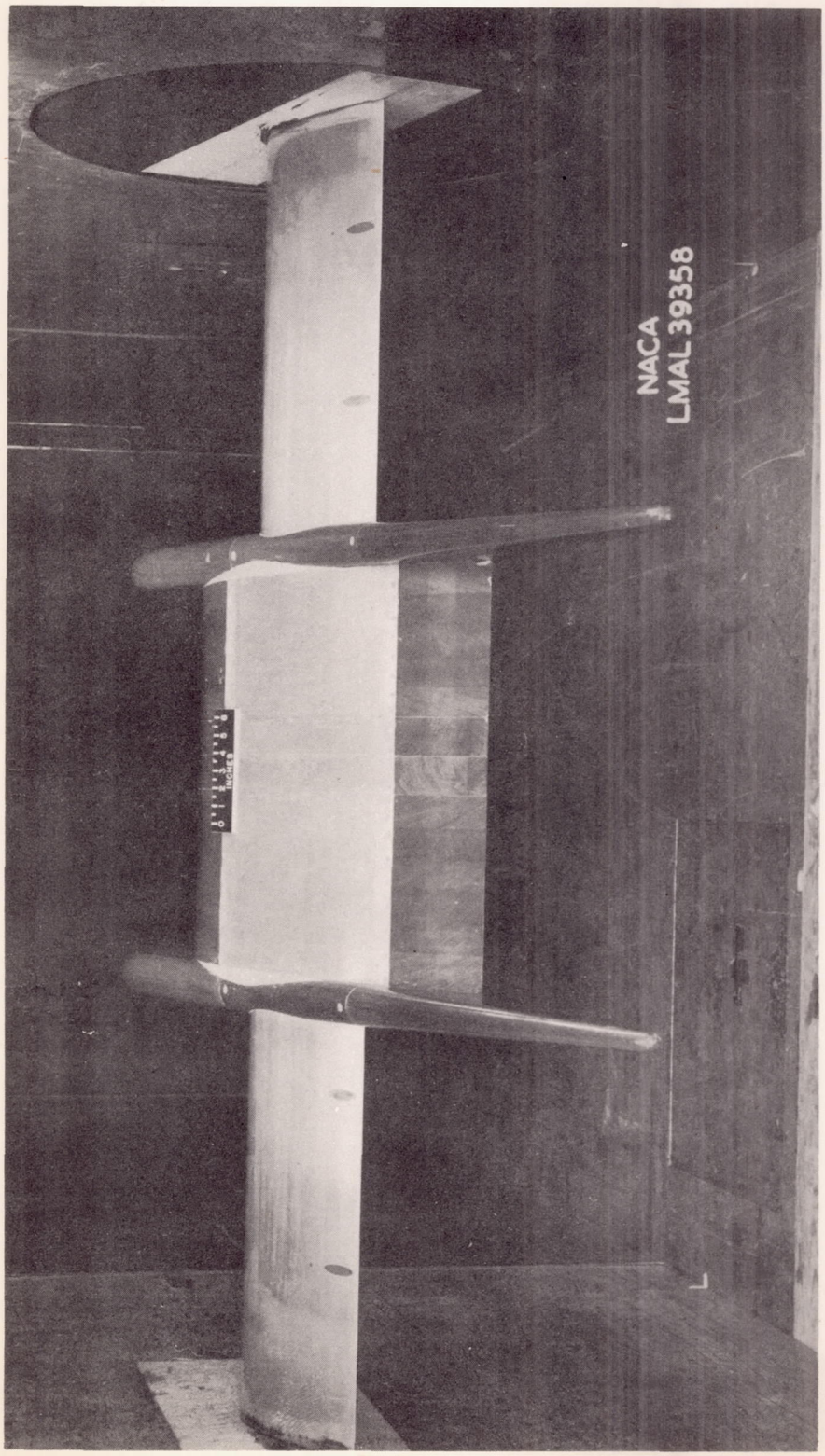

(b) Rear view.

Figure 5.- Concluded.

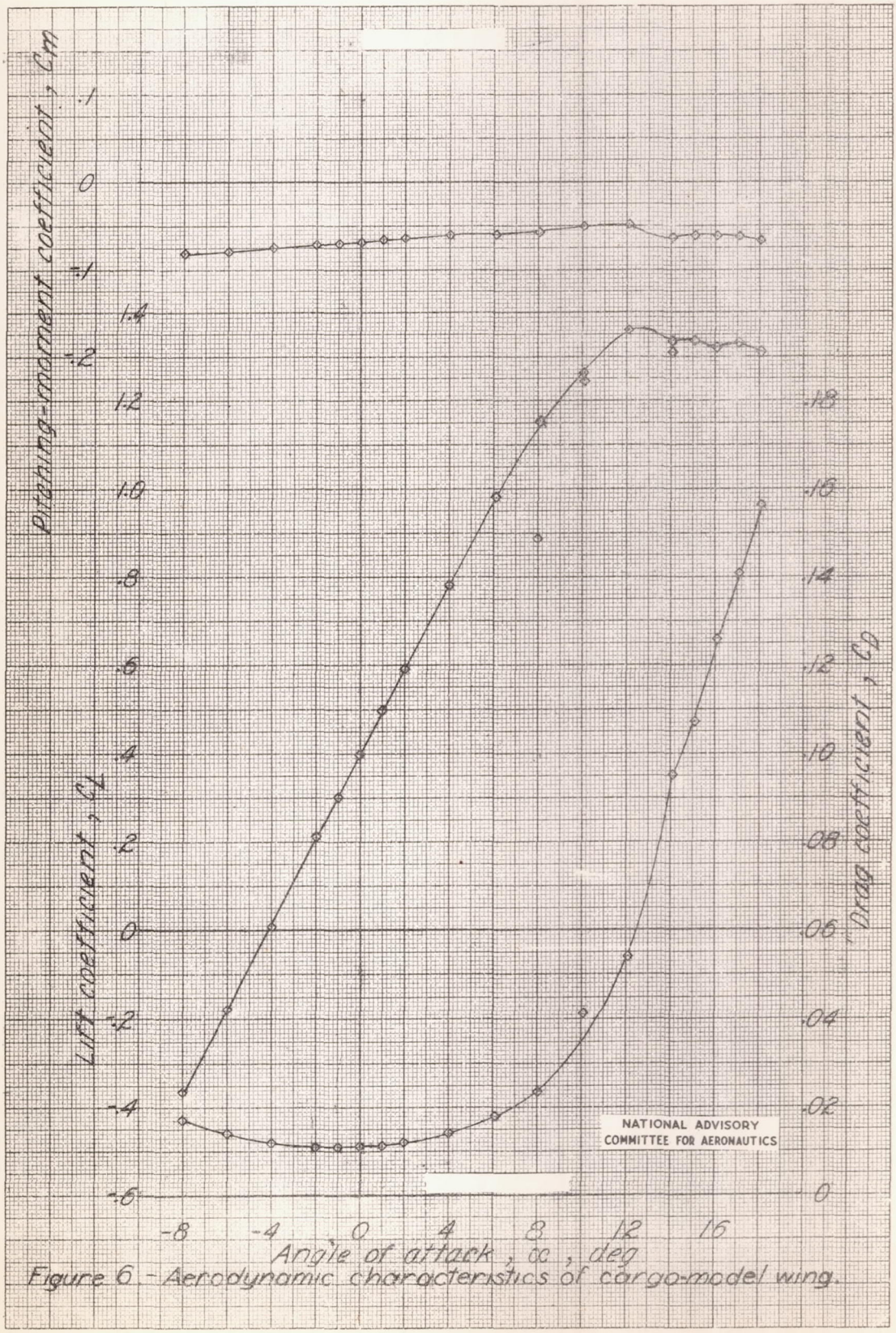

Figure 6.- Aerodynamic characteristics of cargo-model wing.

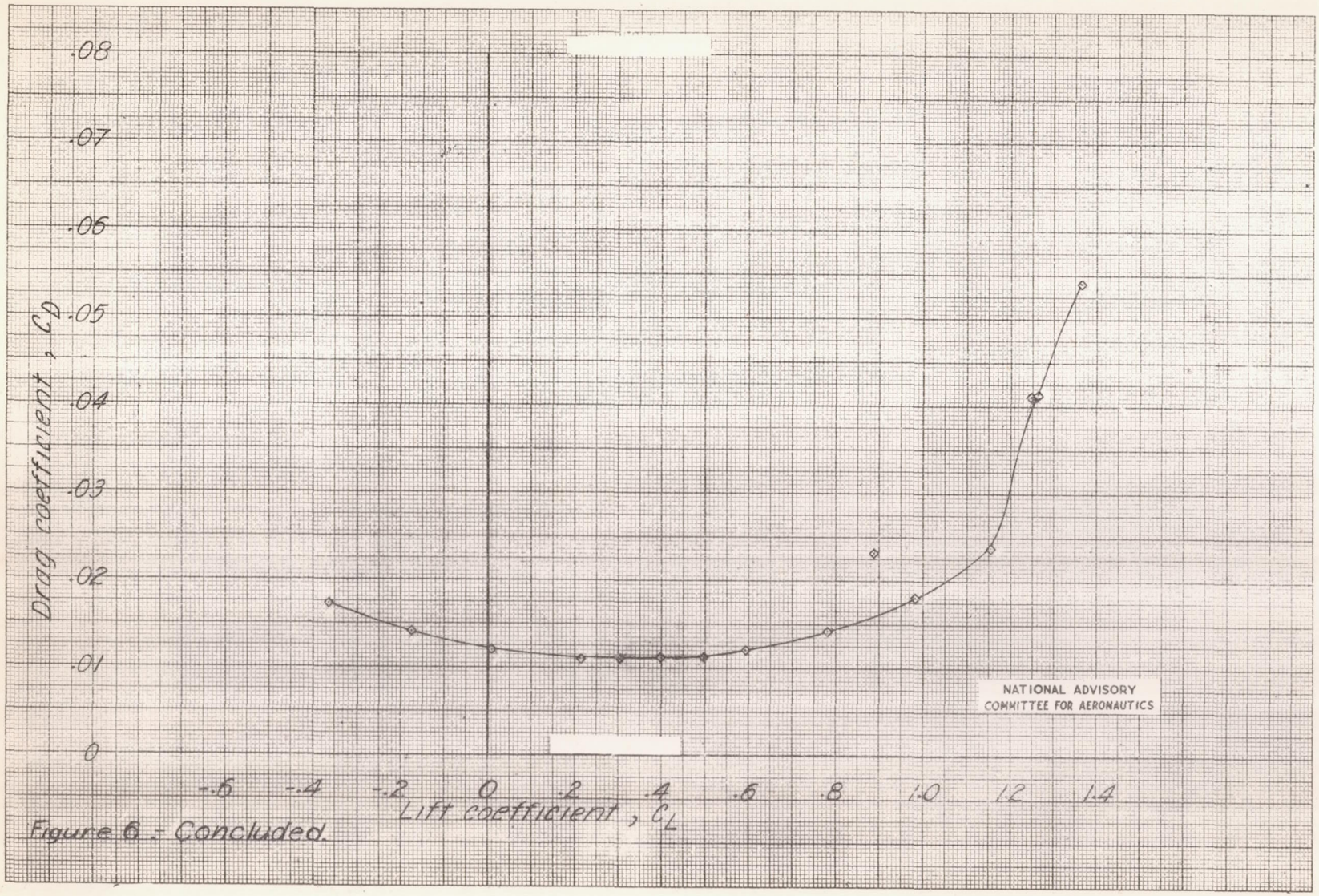

Figure 6.- Concluded.

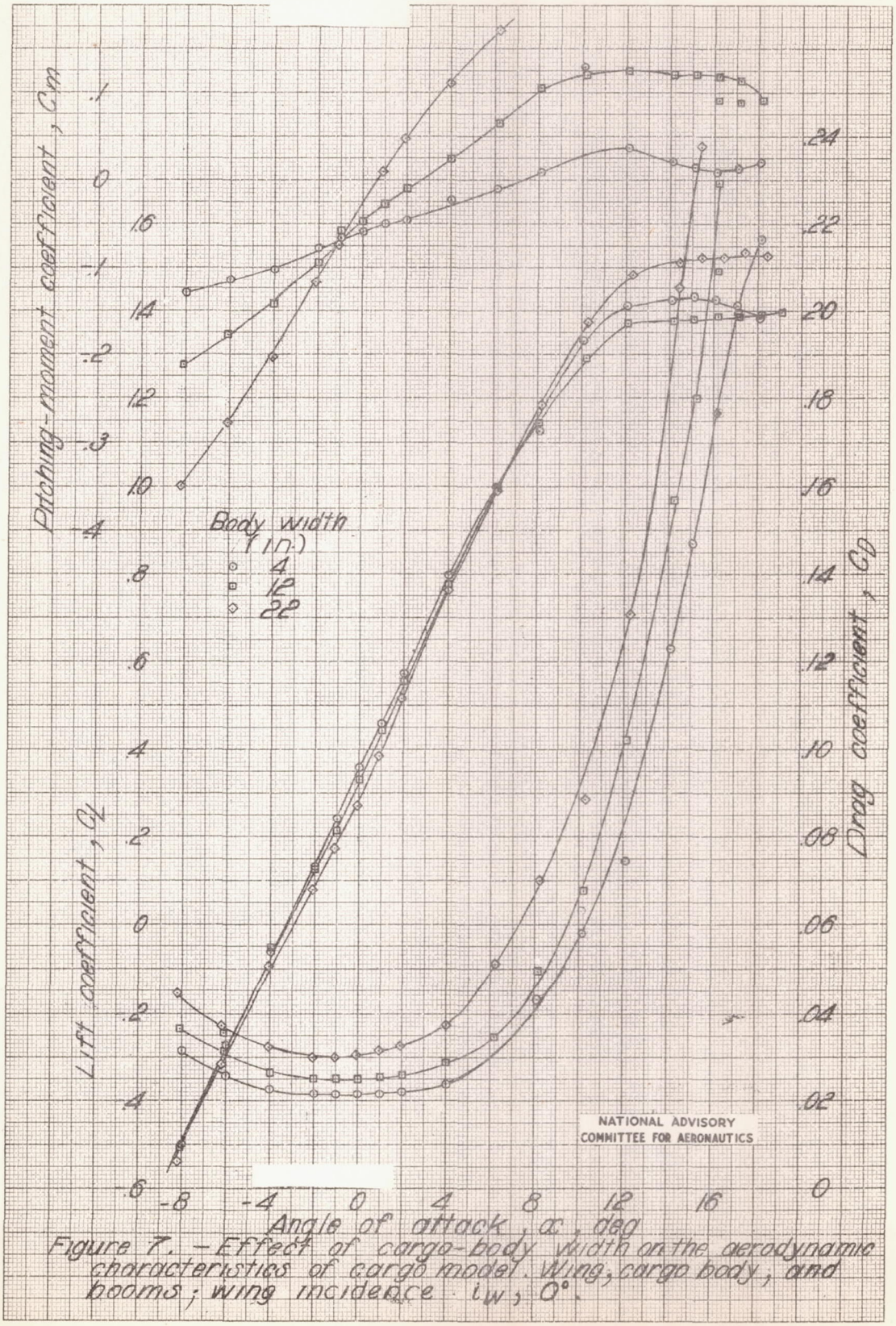

Figure 7. - Effect of cargo-body width on the aerodynamic characteristics of cargo model. Wing, cargo body, and booms; wing incidence i_w, 0°.

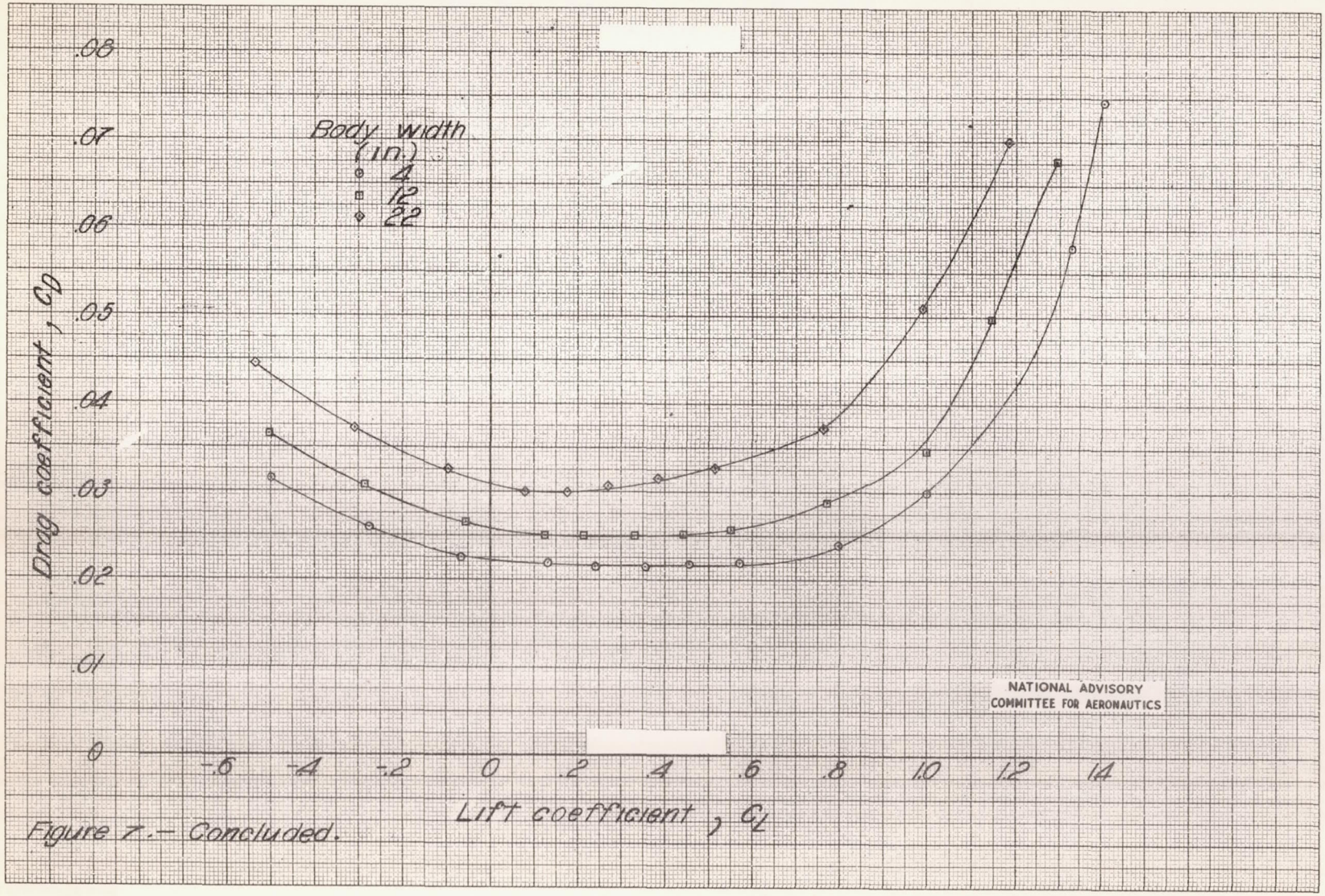

Figure 7.- Concluded.

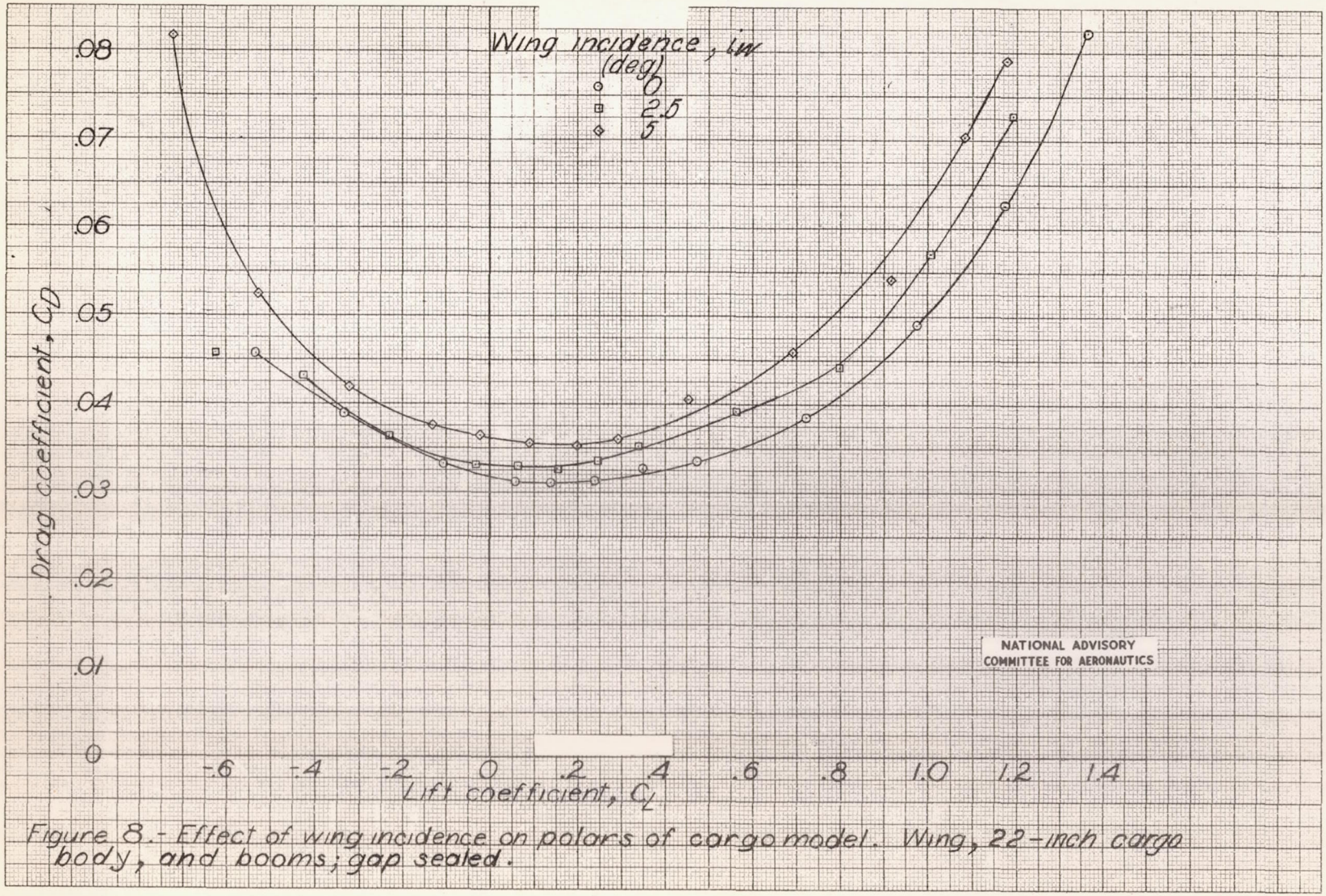

Figure 8.- Effect of wing incidence on polars of cargo model. Wing, 22-inch cargo body, and booms; gap sealed.

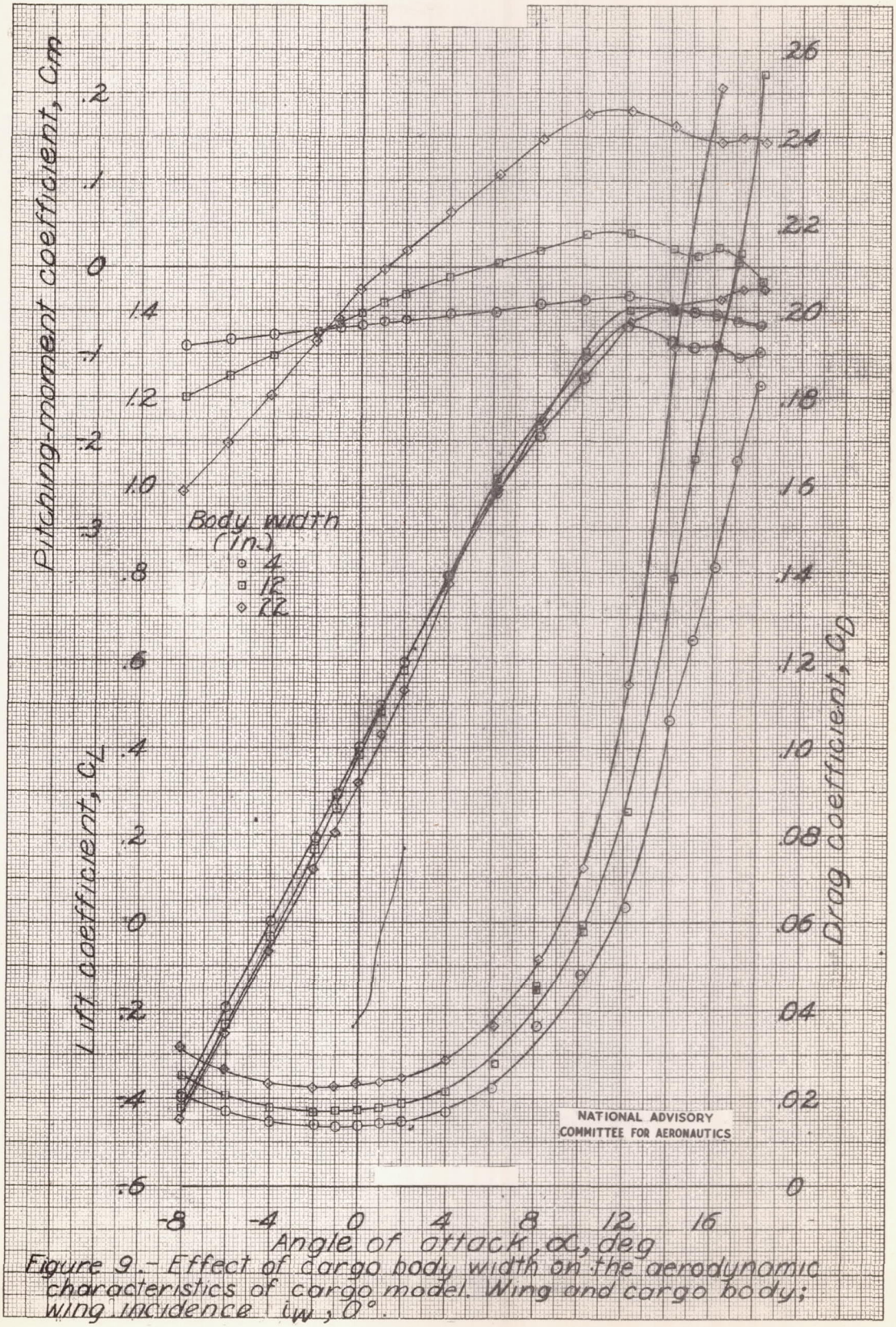

Figure 9.- Effect of cargo body width on the aerodynamic characteristics of cargo model. Wing and cargo body; wing incidence i_w, 0°.

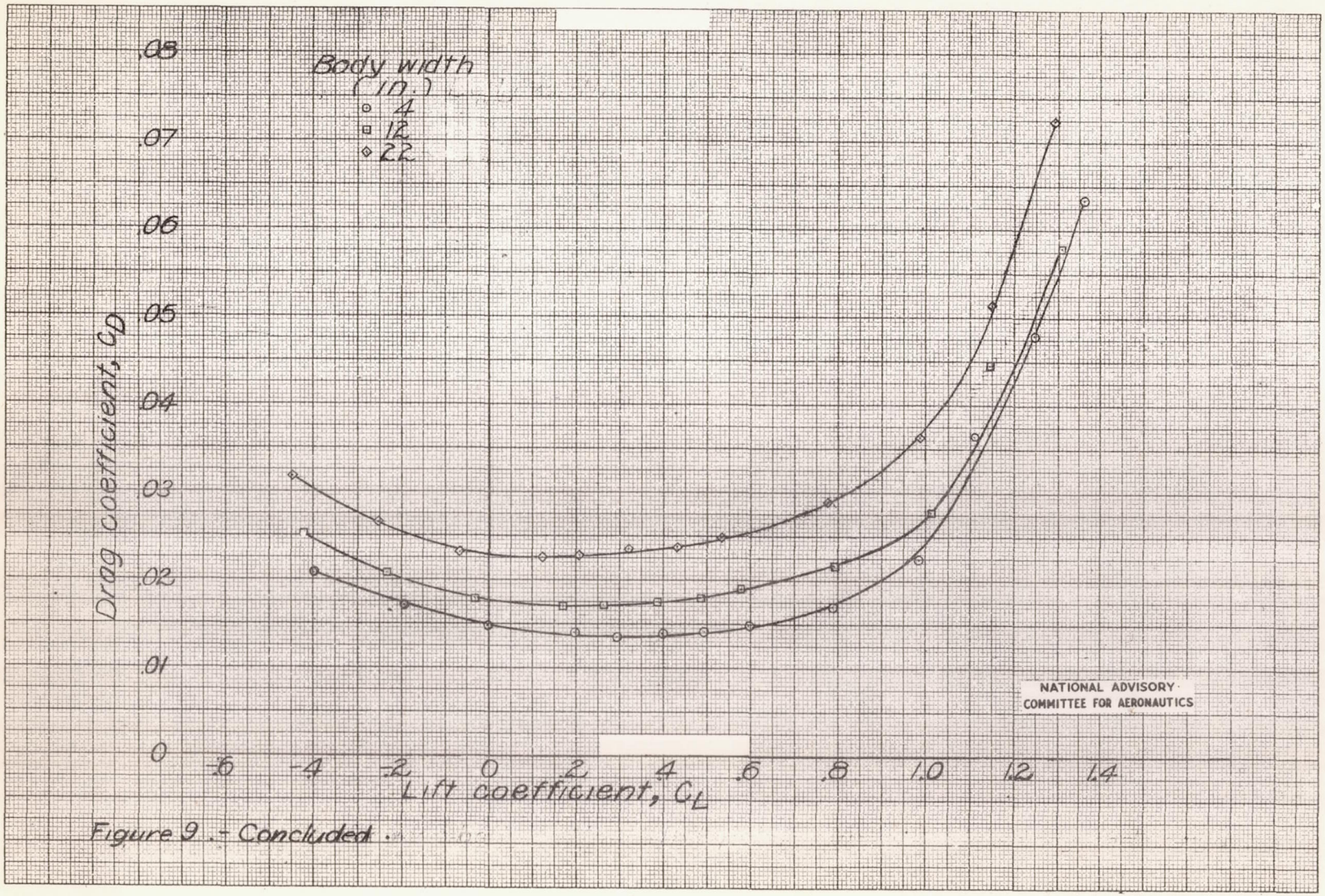

Figure 9.- Concluded.

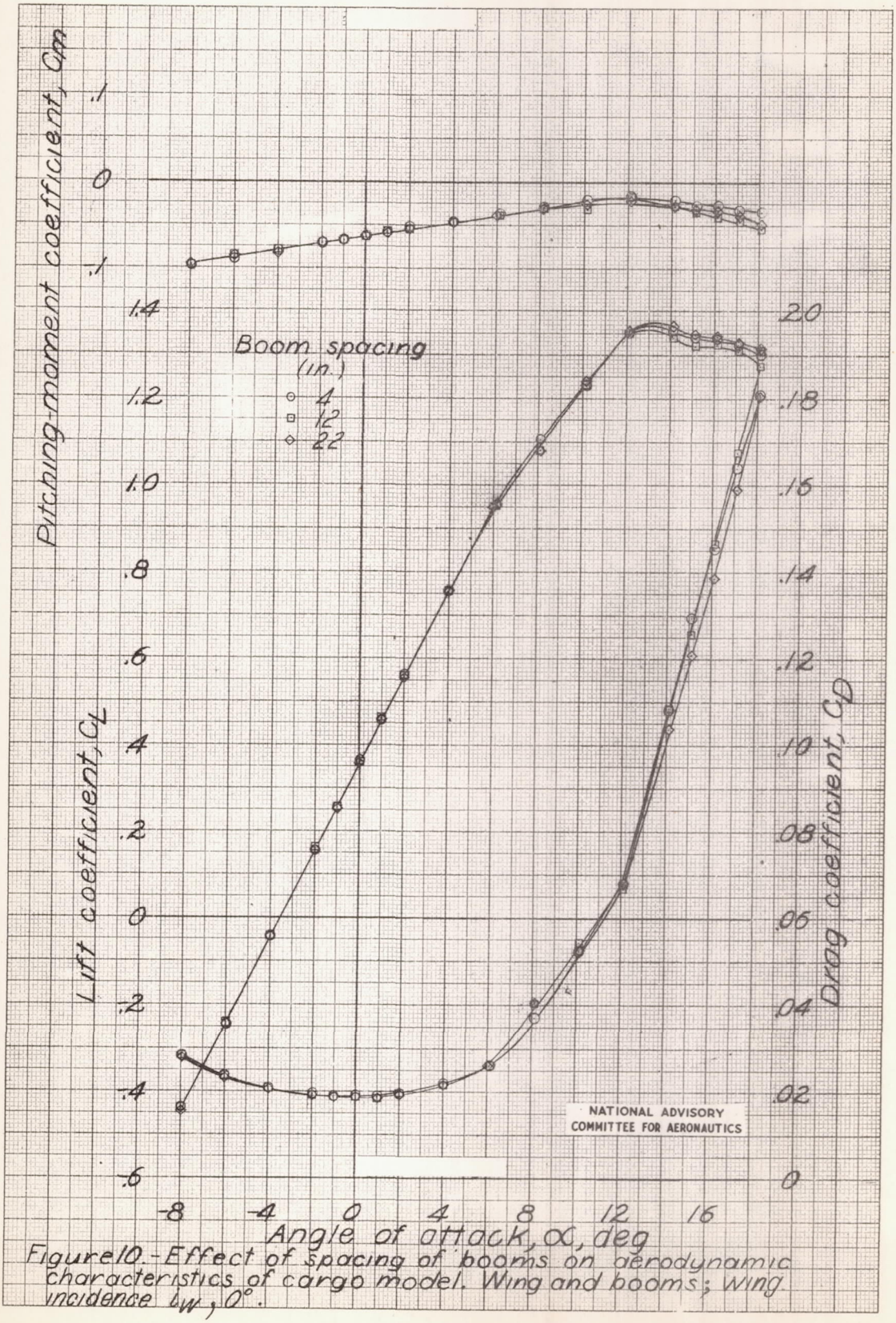

Figure 10.- Effect of spacing of booms on aerodynamic characteristics of cargo model. Wing and booms; wing incidence i_w, 0°.

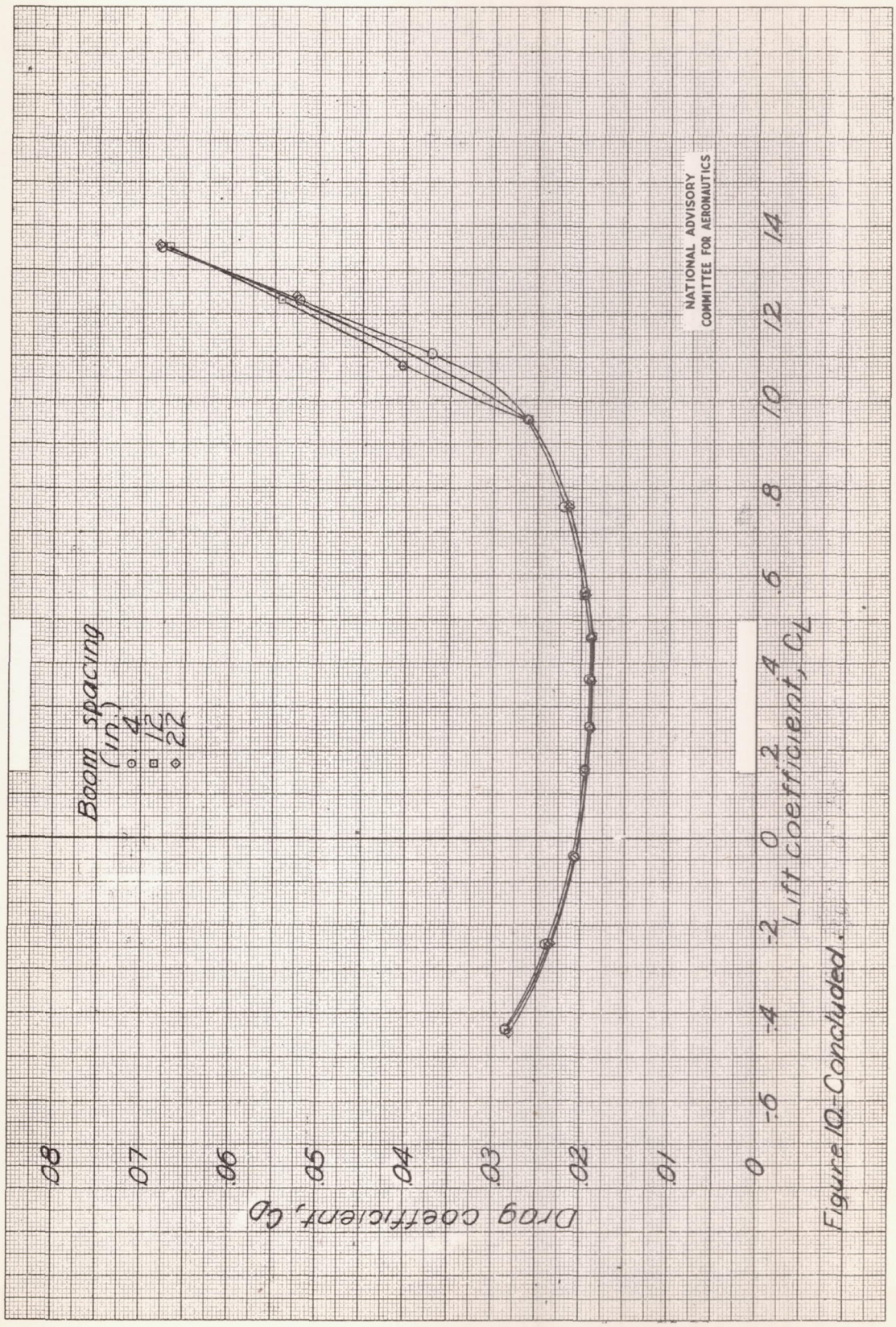

Figure 10.- Concluded.

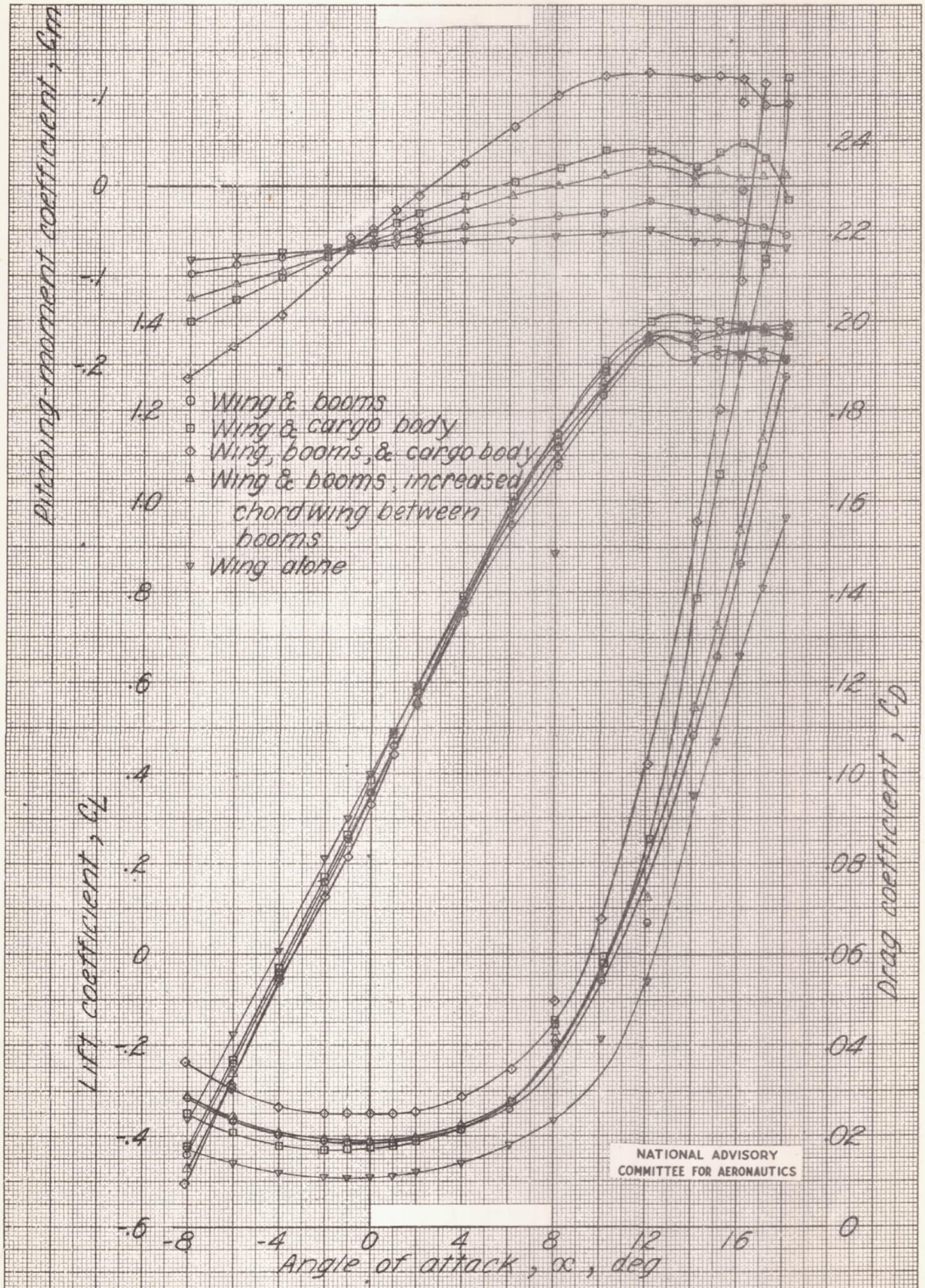

Figure 11.- Aerodynamic characteristics of component parts of cargo model. Arrangement for 12-inch cargo body; wing incidence i_w, 0°.

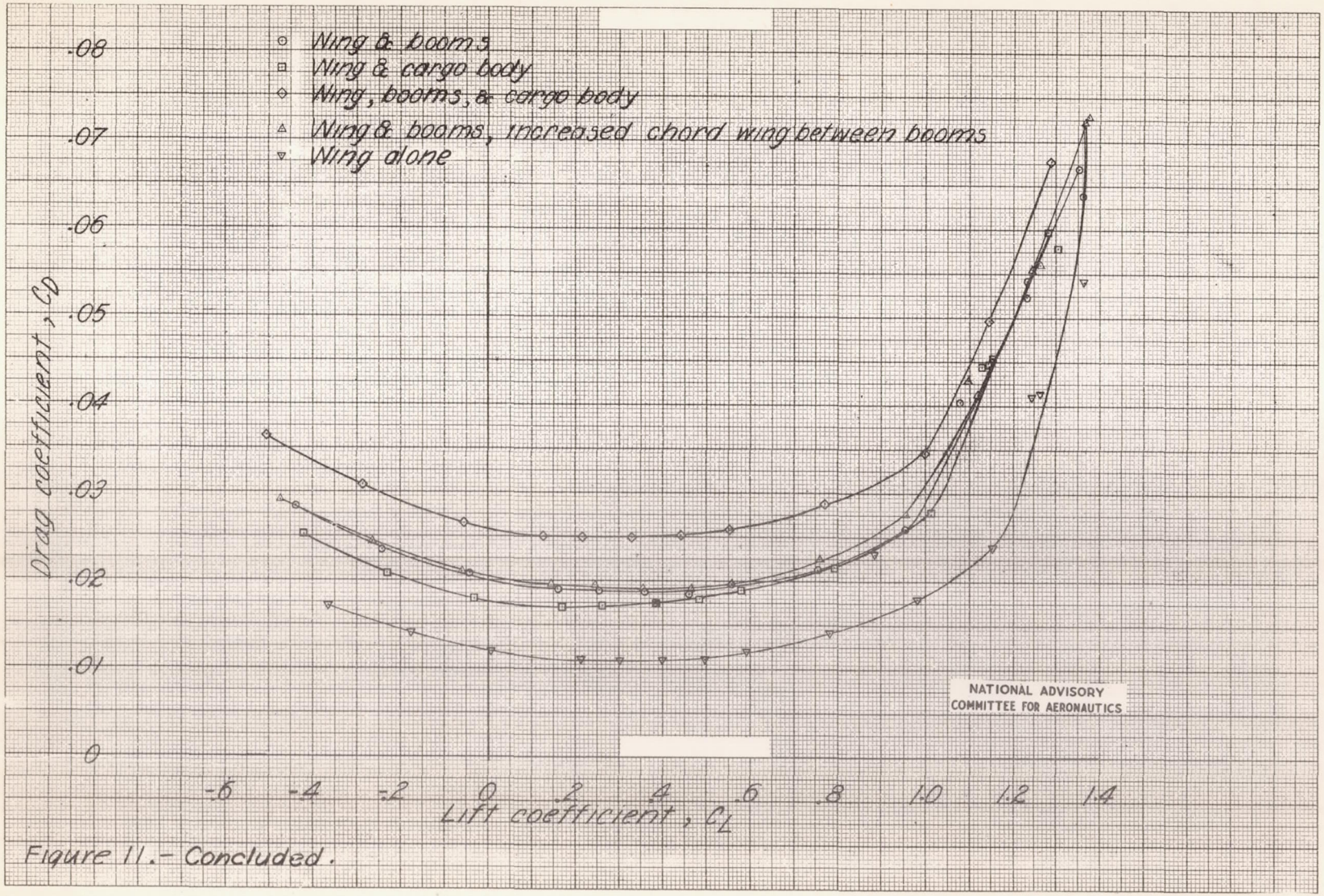

Figure 11.- Concluded.

MR No. L5E09a

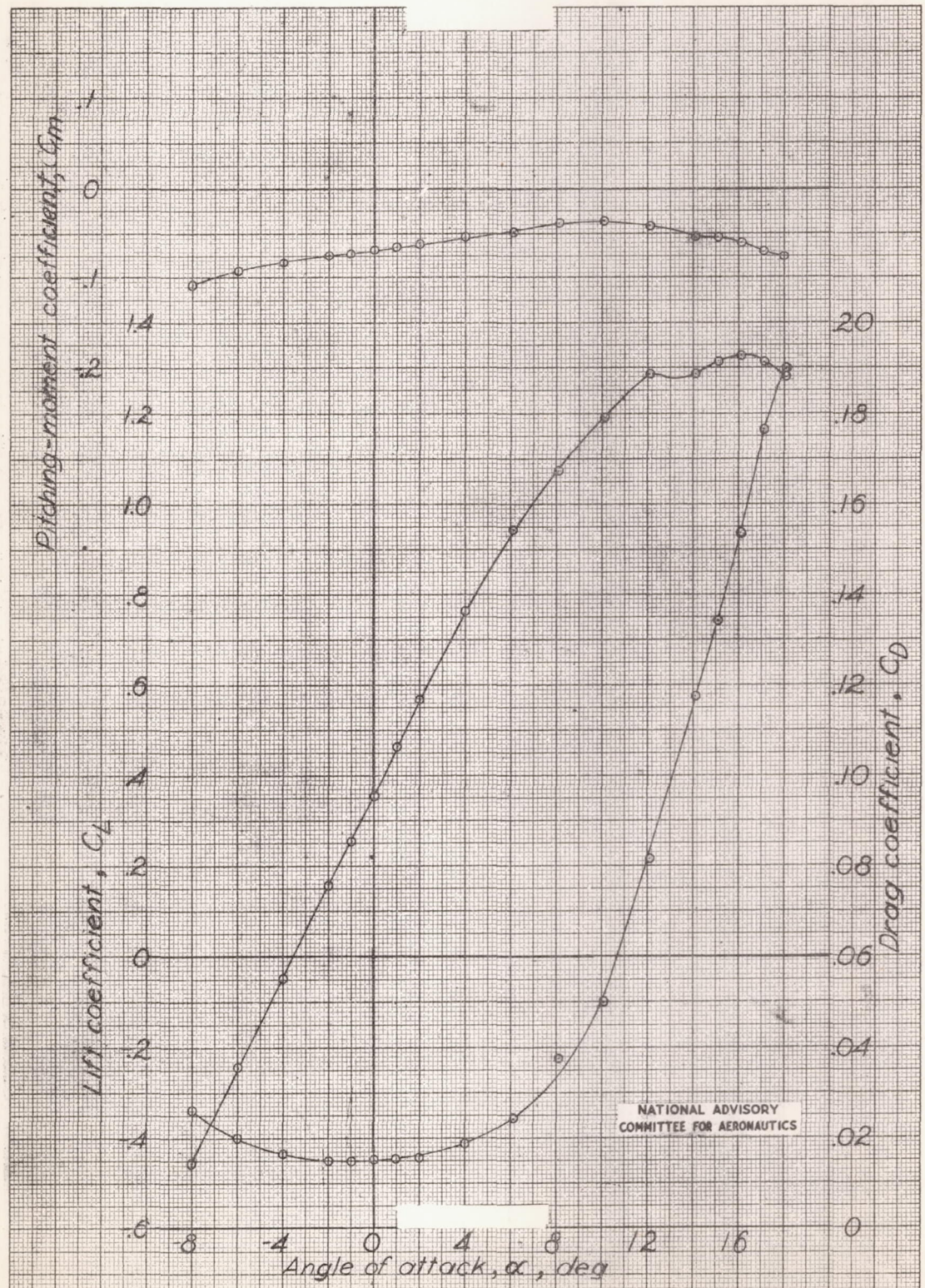

Figure 12.-Aerodynamic characteristics of cargo model. Wing and 5-inch conventional body; wing incidence, i_w, 0°.

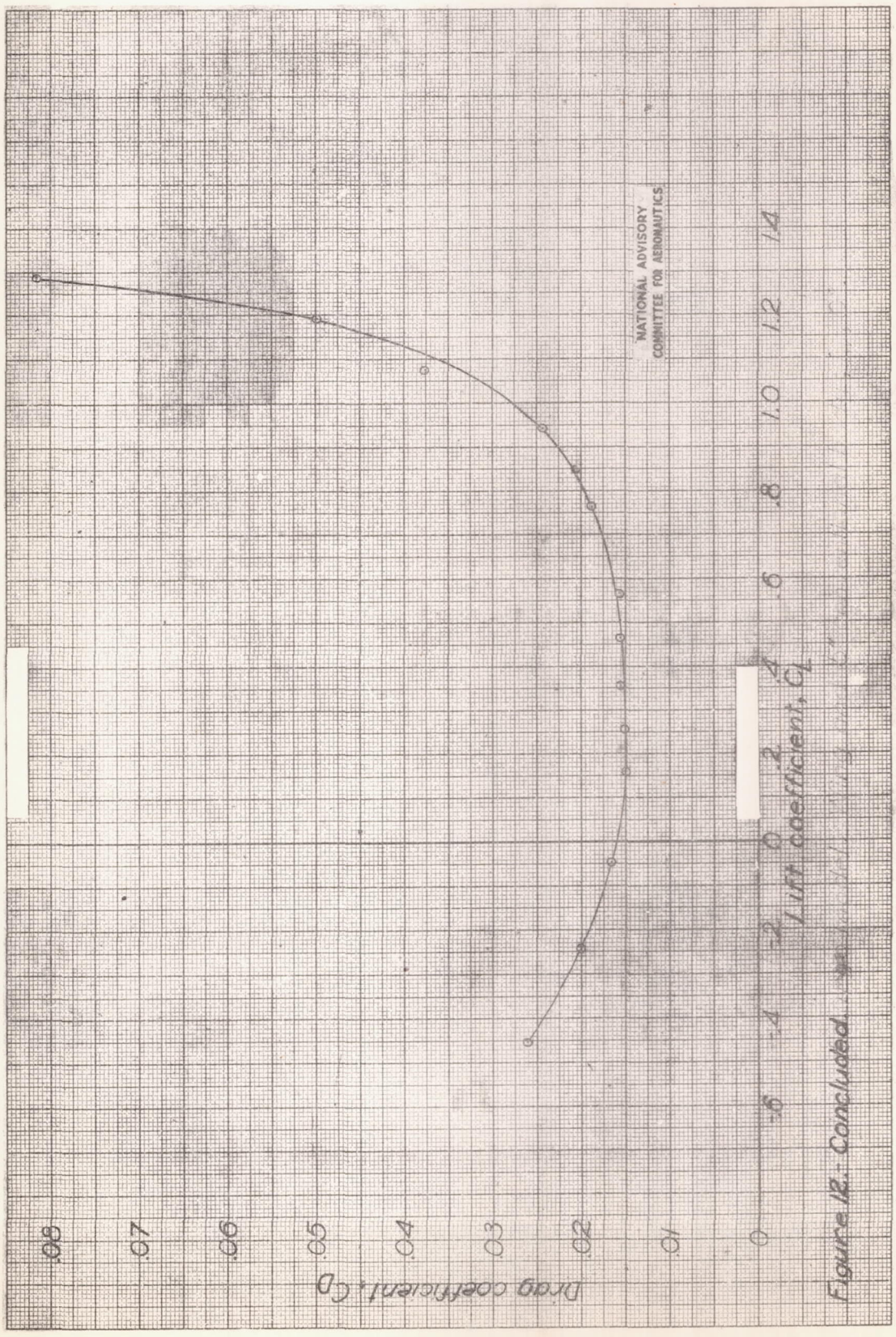

Figure 12.- Concluded.

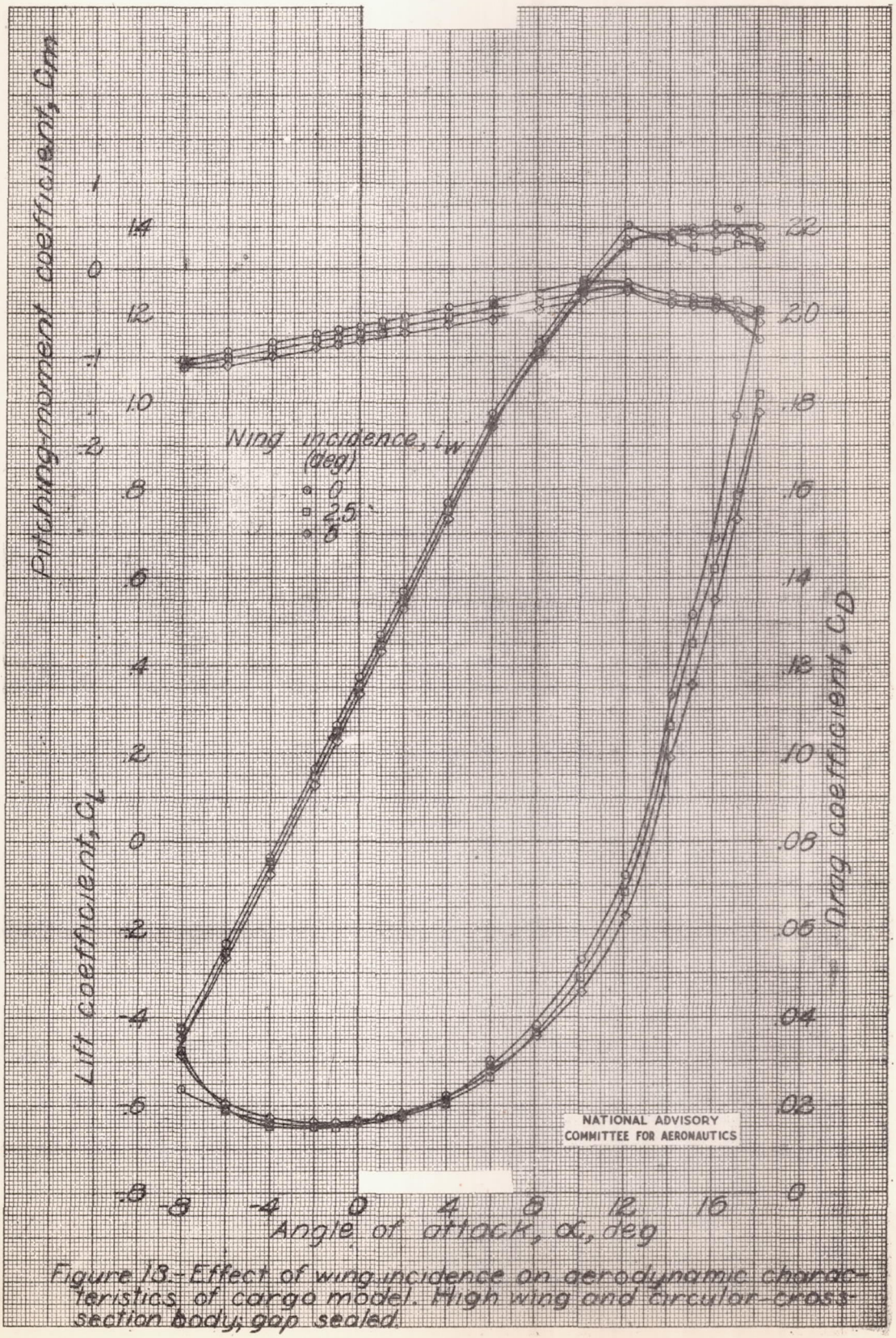

Figure 13.- Effect of wing incidence on aerodynamic characteristics of cargo model. High wing and circular-cross-section body; gap sealed.

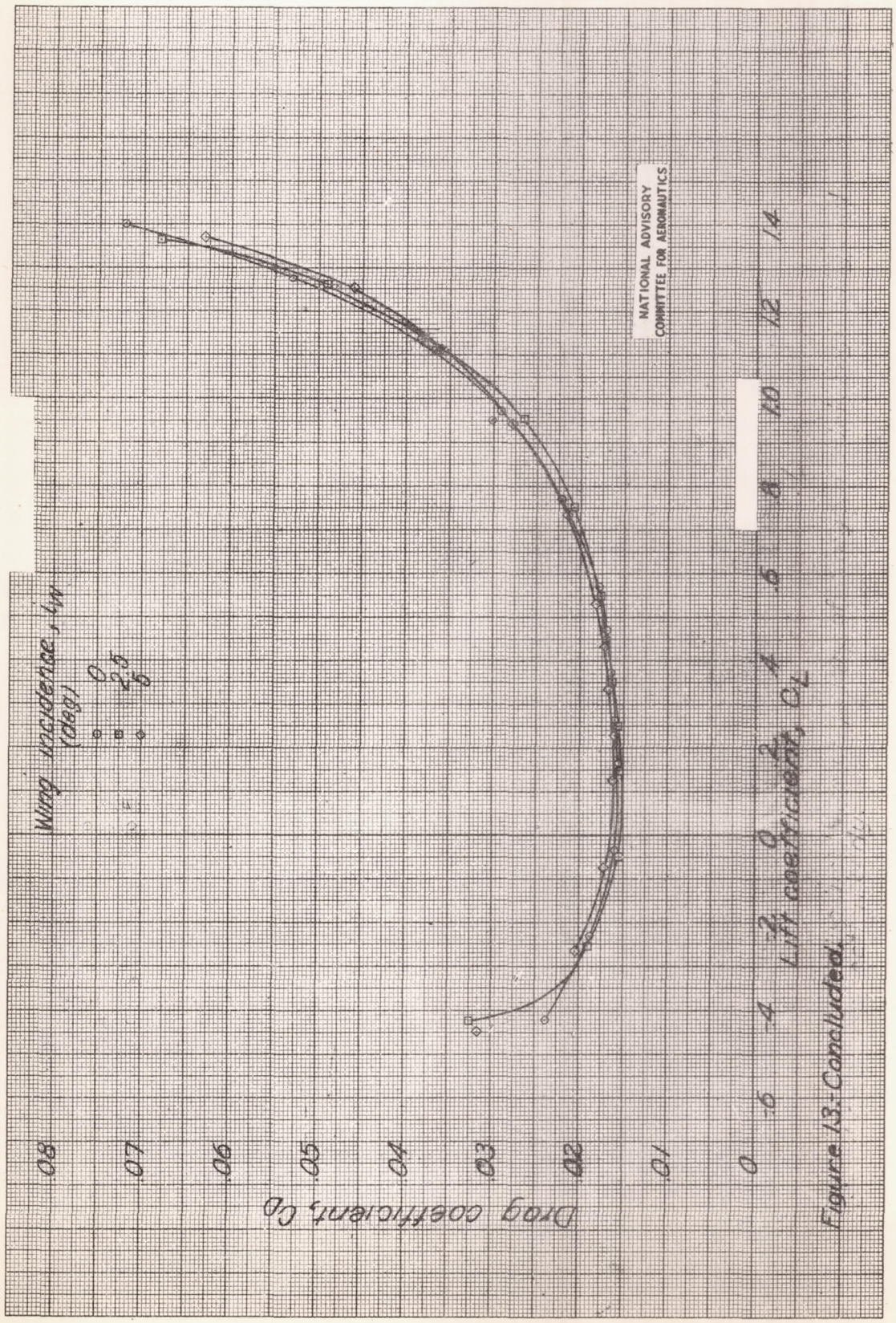

Figure 13.- Concluded.

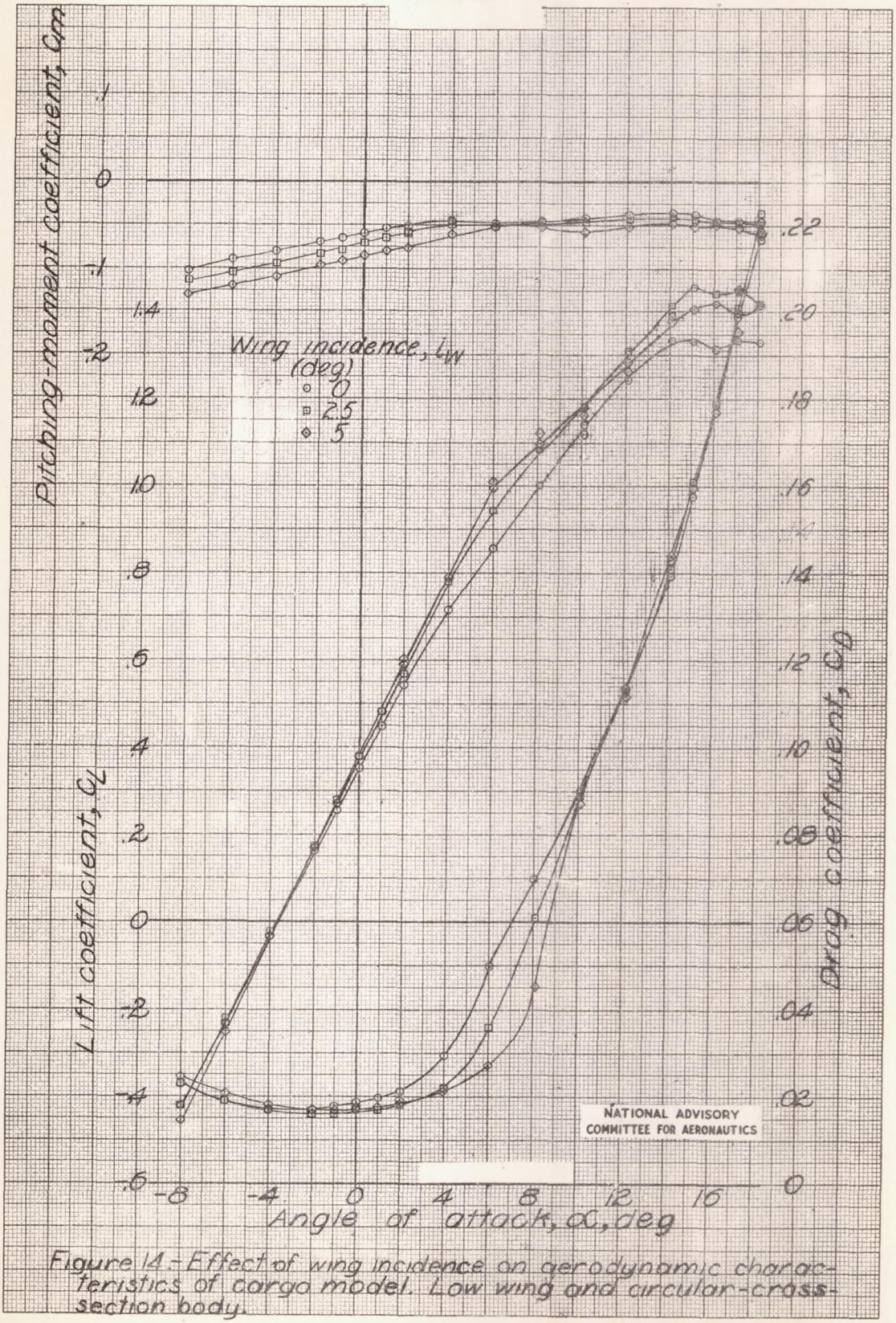

Figure 14.- Effect of wing incidence on aerodynamic characteristics of cargo model. Low wing and circular-cross-section body.

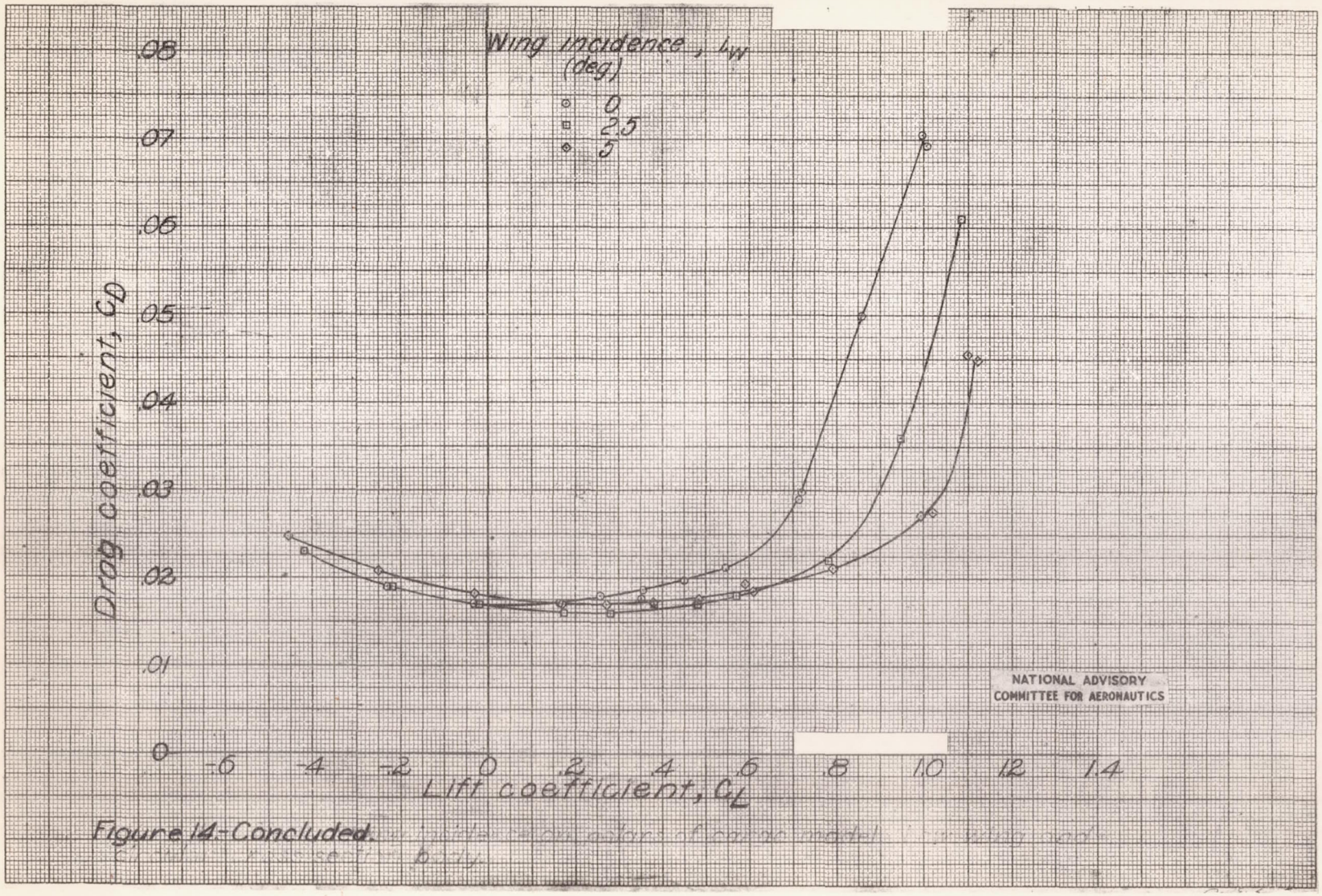

Figure 14.- Concluded.

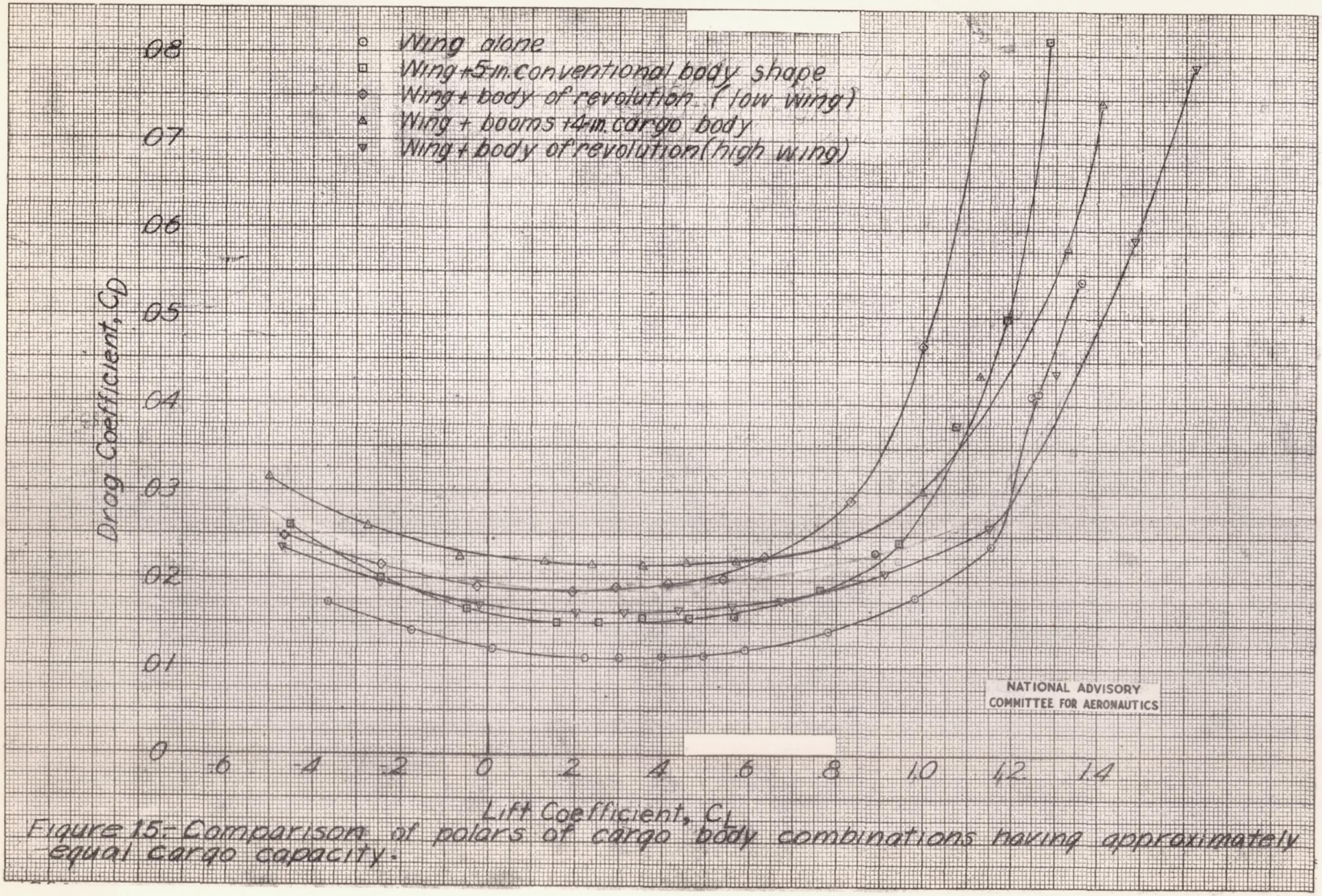

Figure 15- Comparison of polars of cargo body combinations having approximately equal cargo capacity.

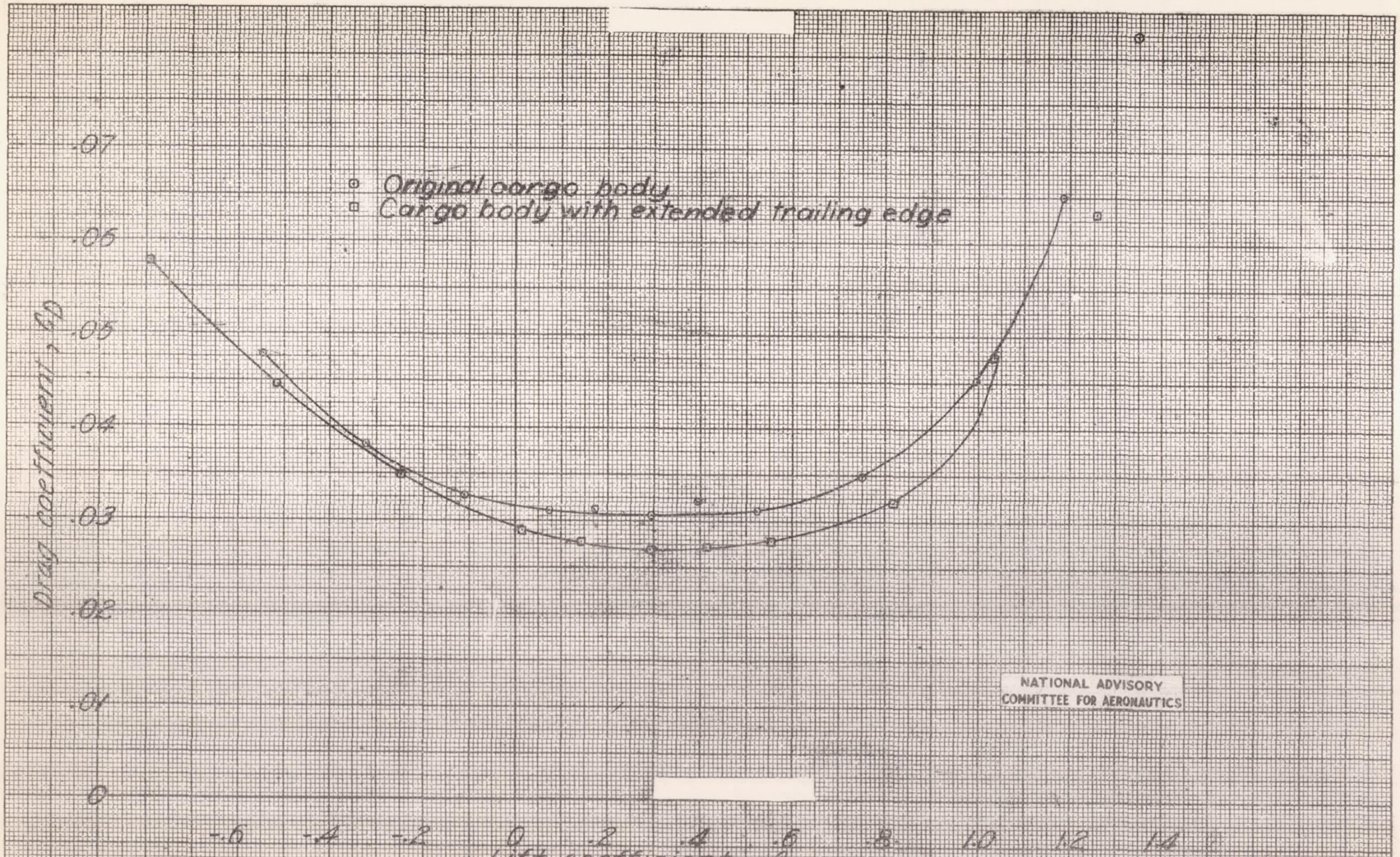

Figure 16.- Effect of extending trailing edge of cargo body on polars of cargo model. Wing, cargo body, and booms; cargo body width, 22 inches; wing incidence, i_w, 0°.

L-541

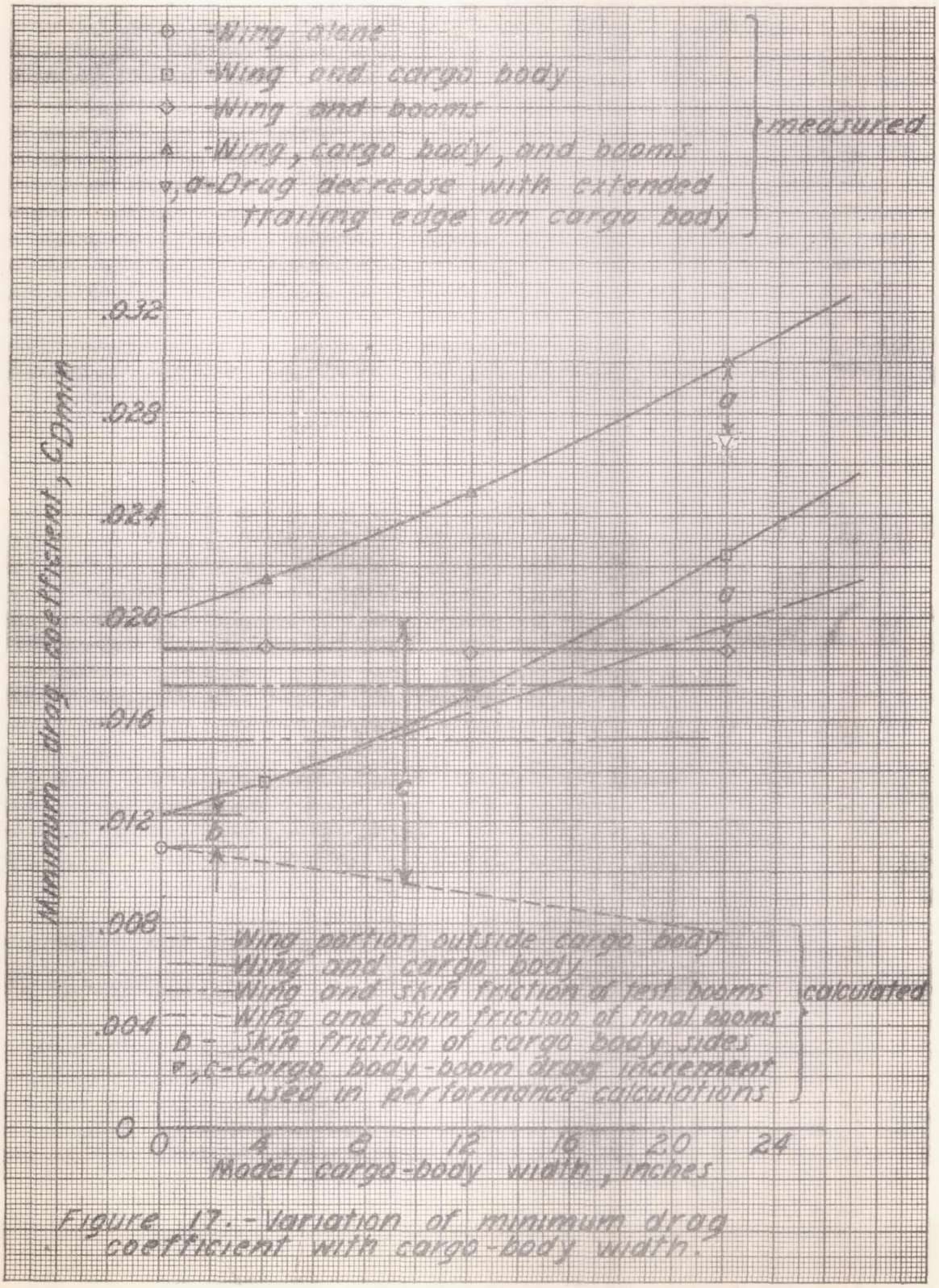

Figure 17.- Variation of minimum drag coefficient with cargo-body width.

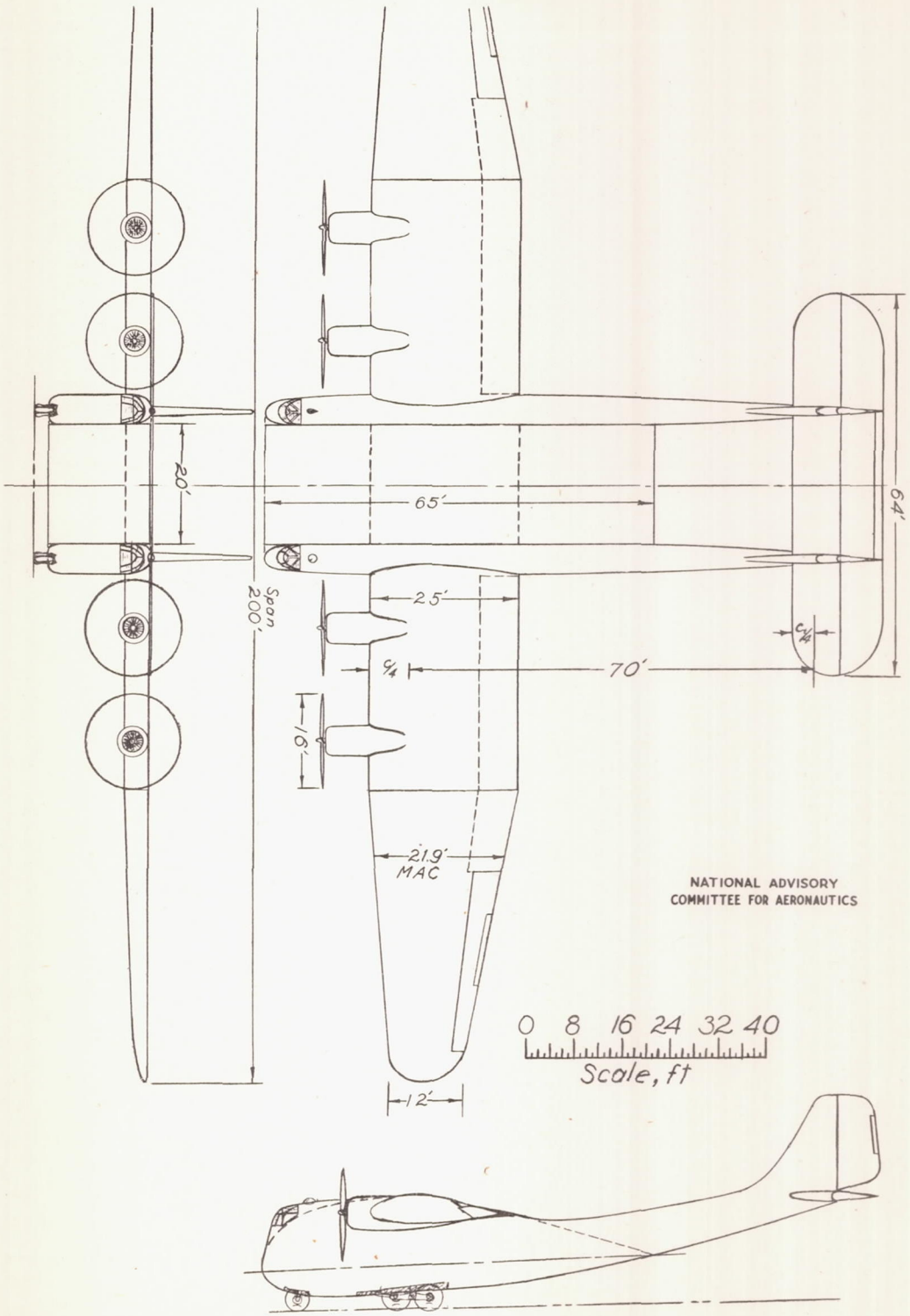

Figure 18.-Three-view drawing of proposed cargo airplane.

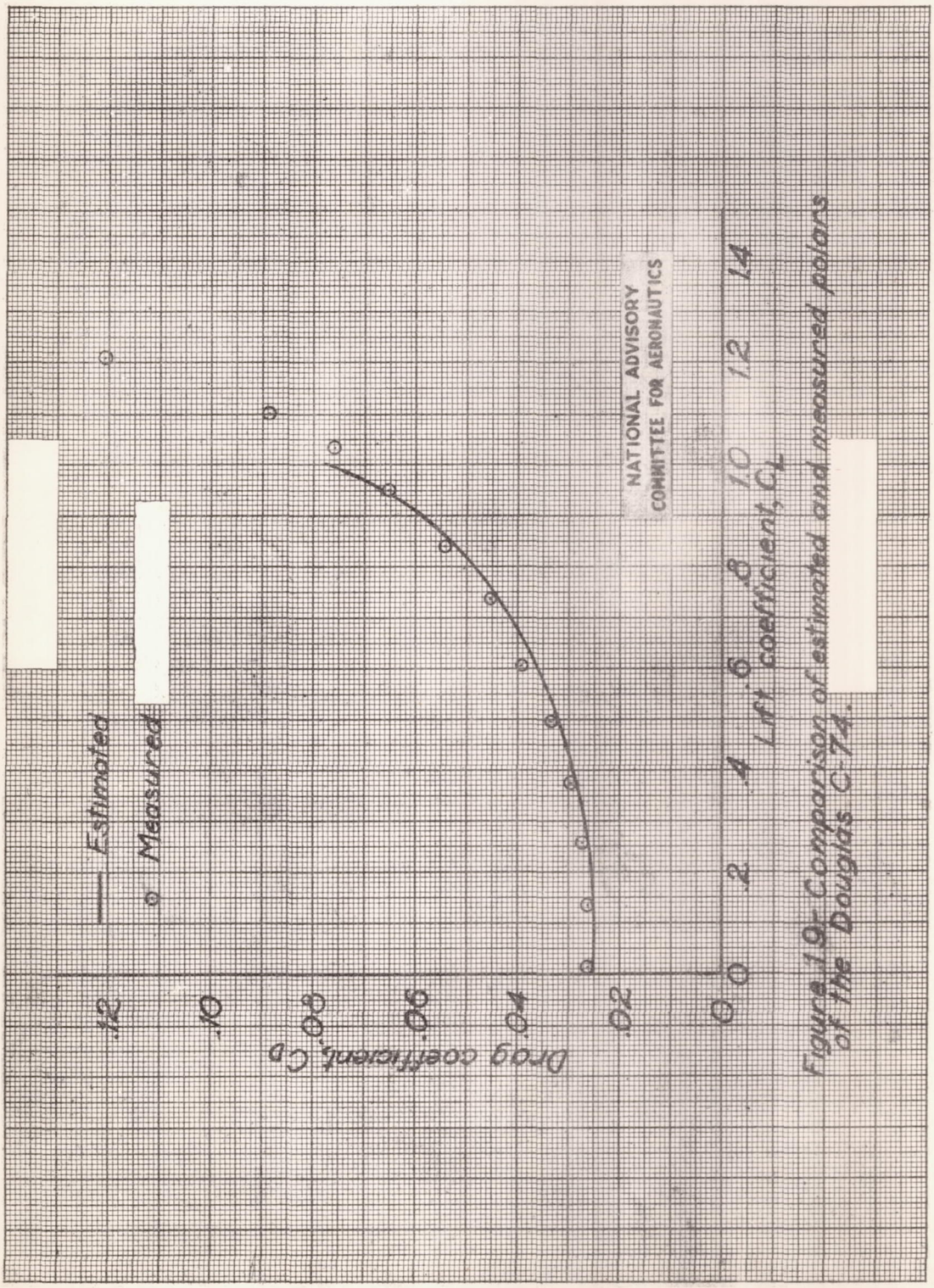

Figure 10.- Comparison of estimated and measured polars of the Douglas C-74.

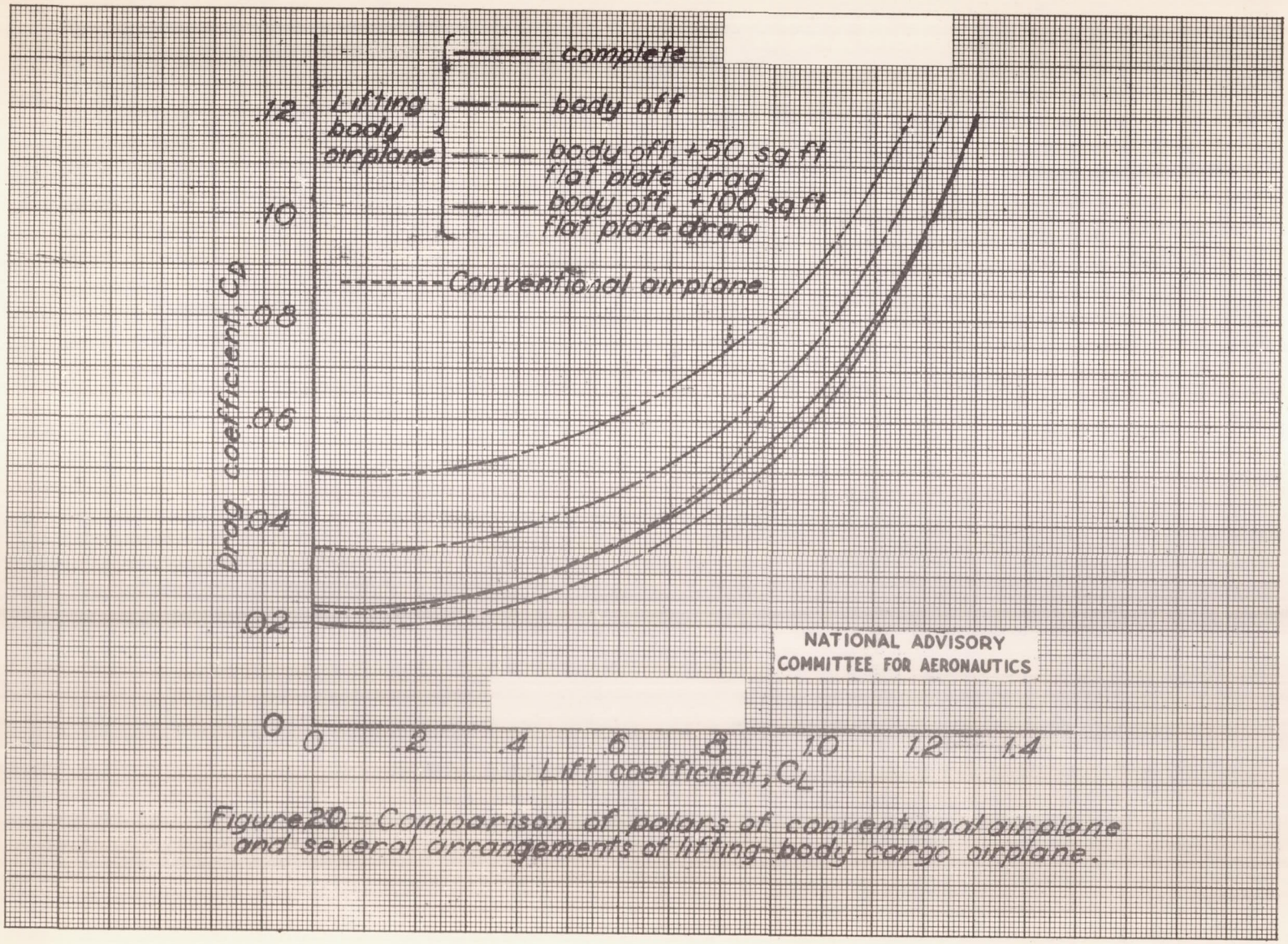

Figure 20.- Comparison of polars of conventional airplane and several arrangements of lifting-body cargo airplane.

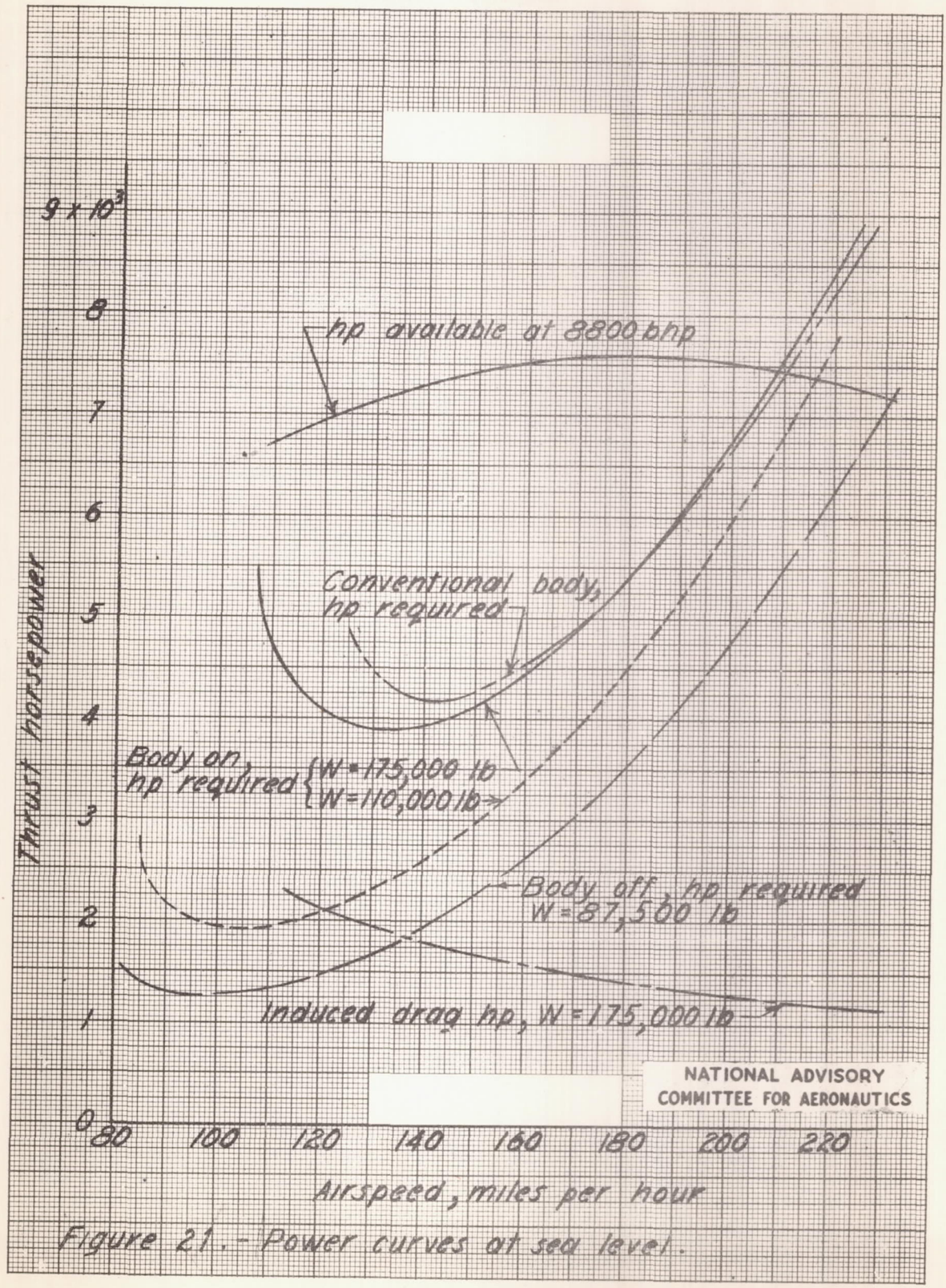

Figure 21.- Power curves at sea level.

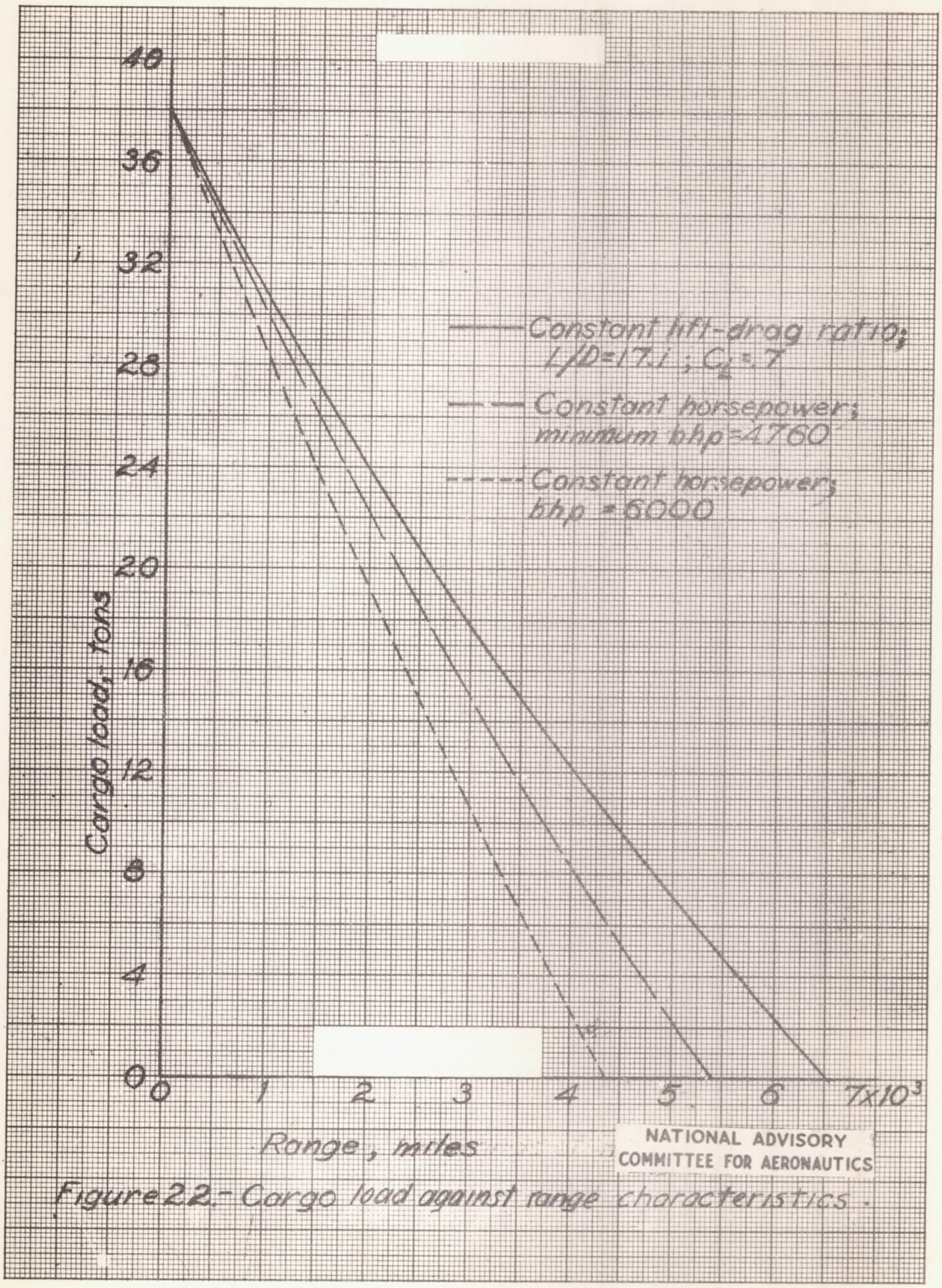

Figure 22.- Cargo load against range characteristics.

L-541

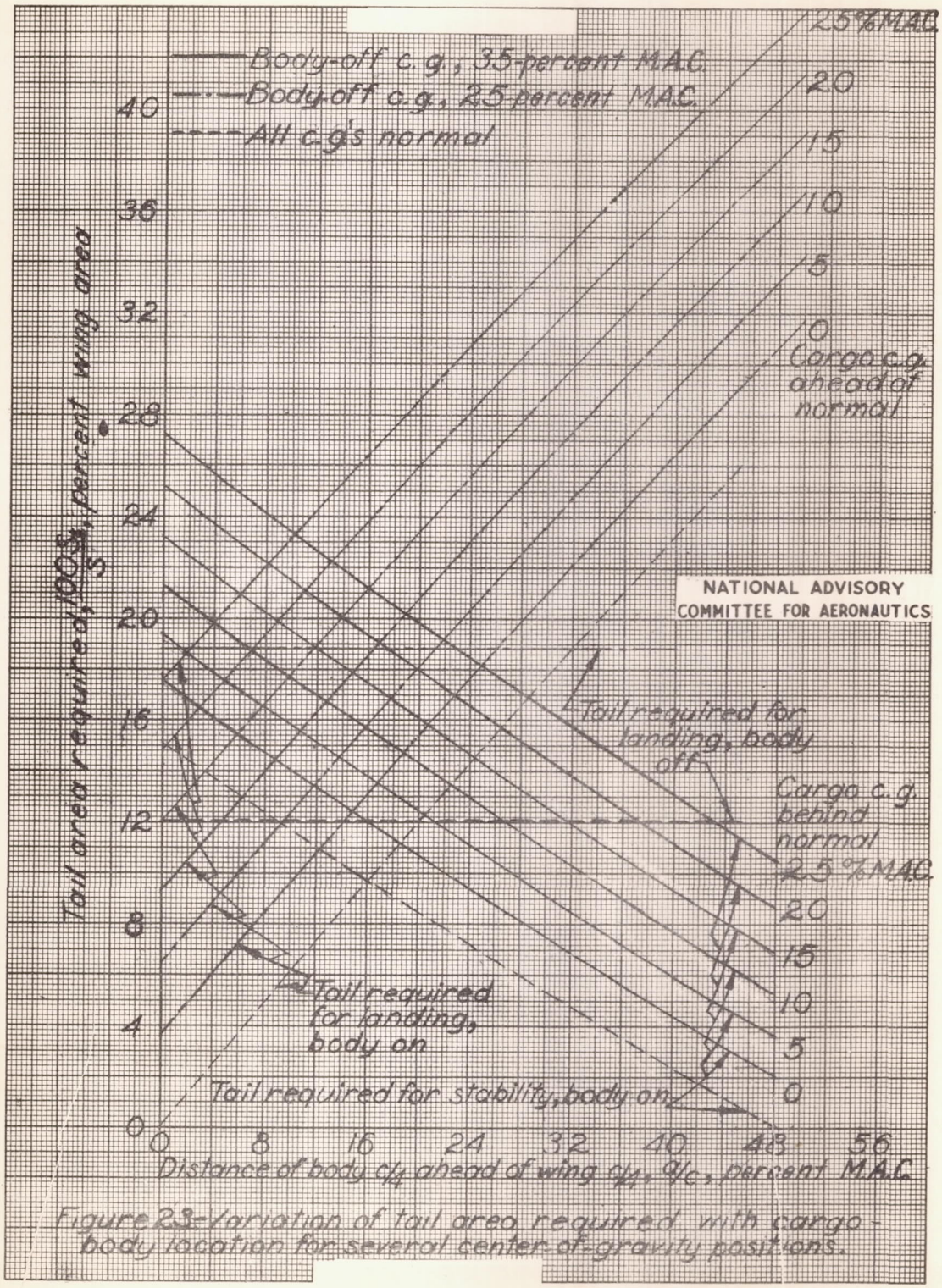

Figure 23-Variation of tail area required with cargo-body location for several center-of-gravity positions.

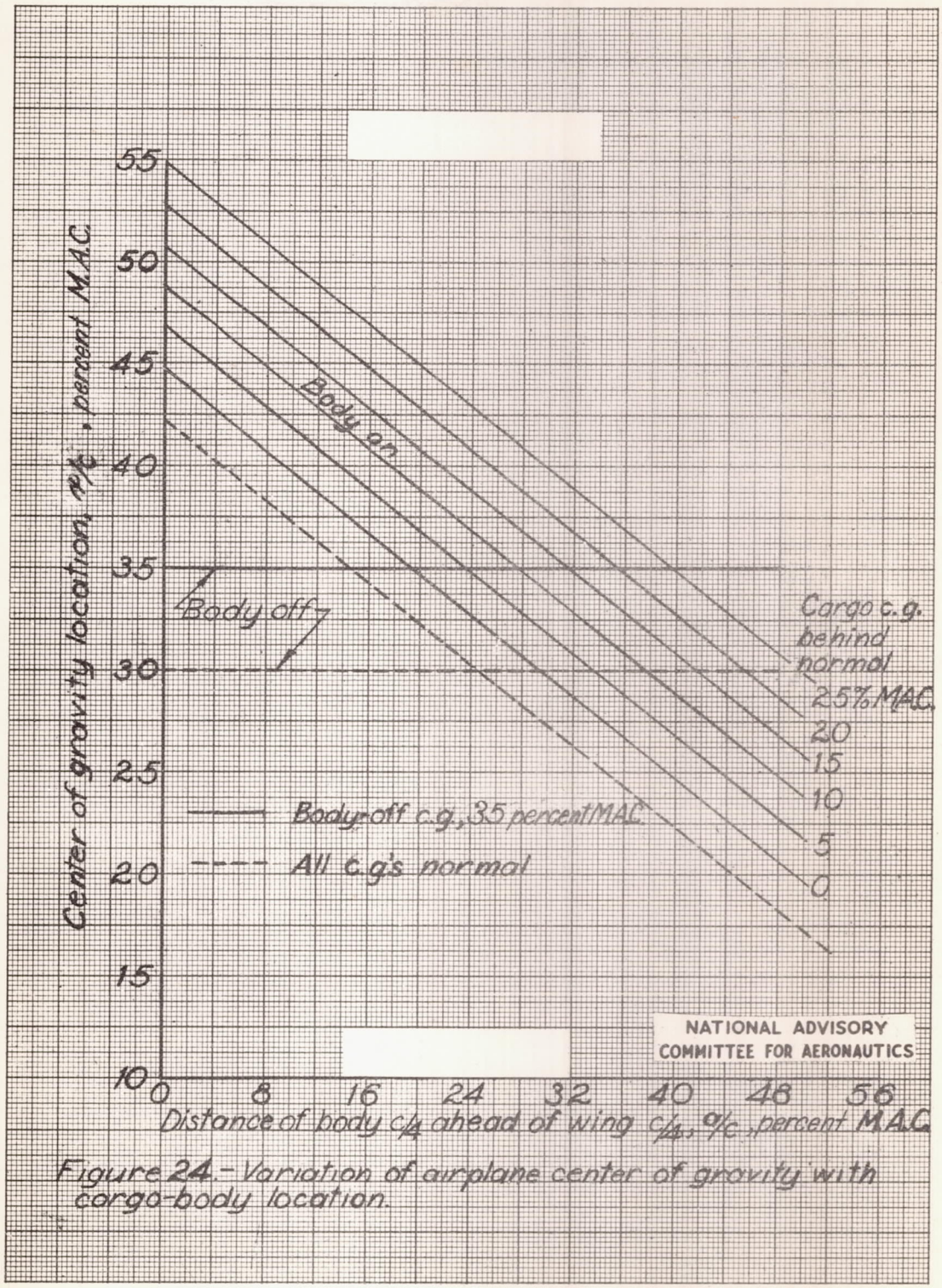

Figure 24.- Variation of airplane center of gravity with cargo-body location.